Sensors & Diagnostics

CRITICAL REVIEW

View Article Online
View Journal | View Issue

Cite this: *Sens. Diagn.*, 2024, **3**, 968

Hydroxypyridinone based chelators: a molecular tool for fluorescence sensing and sensitization

Shalini Singh,[a] Neha Kumari,[a] B. K. Kanungo [b] and Minati Baral *[a]

Received 28th December 2023,
Accepted 5th May 2024

DOI: 10.1039/d3sd00346a

rsc.li/sensors

Among the currently developed analytical tools, sensors based on fluorescence detection have received immense recognition owing to their high sensitivity, low cost, fast response, and simplicity. The design and synthesis of fluorescence chemosensors to sense metals that are of environmental and biological relevance are of appreciable interest. The efficacy of fluorescent sensors relies on two crucial features: a metal binding unit and a fluorophore that can absorb and emit light. The electronic structure of the sensor is altered upon complexation, leading to a change in light emission or absorption intensity and wavelength. Hydroxypyridinones, a class of N-heterocyclic metal chelators, are appreciated as magnificent chemical tools in metal chelation with a higher affinity towards hard metals, displaying various medical, biological, and industrial applications. However, such compounds are scarcely used as sensors. This article outlines the recent invention of fluorescence chemosensors related to hydroxypyridinone based chelators for the selective sensing of analytes of biological and environmental importance. This discussion involves the structural parameters, coordination mode, and other approaches that helped develop highly selective fluorescence sensors for the ions. In addition, the luminescence properties of the hydroxypyridinones in the energy transfer process of lanthanide chelates as sensitizers are determined.

Introduction

Hydroxypyridinones (HOPOs) are an essential class of N-heterocyclic chelators containing dioxo ligands, considered "privileged" structures for drug design.[1,2] Easy derivatization to regulate the bioavailability with low toxicity has attracted more interest in these chelators. They are classified into three categories, named as, 1-hydroxy-2-pyridinones (1,2-HOPOs), 3-hydroxy-2-pyridinones (3,2-HOPOs), and 3-hydroxy-4-pyridinones (3,4-HOPOs).[3] Fig. 1 represents the structures of these classes of HOPOs.

HOPO-based chelators are recognized for their outstanding chelation properties and their selectivity towards

[a] *Department of Chemistry, National Institute of Technology, Kurukshetra, Haryana 136119, India. E-mail: minatibnitkkr@gmail.com*
[b] *Department of Chemistry, Sant Longowal Institute of Engineering and Technology, Longowal, Punjab-148106, India*

Shalini Singh

Shalini Singh received her M.Sc. degree in chemistry from Kurukshetra University, Haryana, India. She is pursuing her Ph.D. degree under the supervision of Prof. Minati Baral at the National Institute of Technology, Kurukshetra, after being awarded a Junior Research Fellowship in chemical sciences by the University Grants Commission, India. Her major research interests include the synthesis of biomimetic chelators and their complexes with transition metal ions and lanthanoids, metal ion sensing and computational chemistry.

Neha Kumari

Neha Kumari completed her B. Sc. (Medical) degree in 2016 and received her Master's degree in Chemistry in 2018 from Savitribai Phule Pune University, Pune, Maharashtra, India. Following her academic achievements, she joined as a Ph.D. scholar in the Department of Chemistry at National Institute of Technology, Kurukshetra, Haryana, India under the supervision of Prof. Minati Baral. Her research interest includes inorganic synthesis, metal complexation, metal ion sensing and theoretical studies.

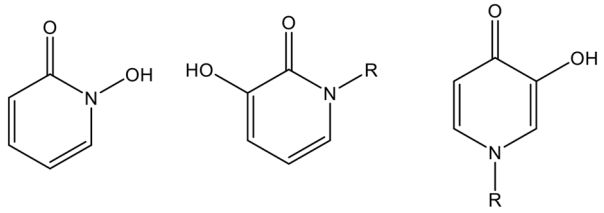

Fig. 1 Structures of different classes of HOPOs namely, 1,2-HOPO; 3,2-HOPO, and 3,4-HOPO.

a range of metal ions. These chelators possess a prominent effect on sensitivity and selectivity to the target metal ions by allowing the attachment of a HOPO unit which produces a five-membered stable ring. The selectivity and sensitivity of any chelator towards metal ions can be affected by various parameters including ring size, ionic radii, hardness and softness character, attainment of stability and (or) rigidity, *etc.* The coordination number, net ionic charge, and stereochemistry of the molecules are among some of the important parameters that are mainly considered while designing a chelator. The selectivity of hydroxypyridinone-based chelators for specific metal ions is justified by introducing the concept of "hard" or "soft" acids and bases. Having two hard oxygen donors for coordination, HOPO-based ligands possess high affinity towards hard metal ions. The design of new multidentate chelators demonstrating high selectivity and sensitivity is based on the factors described above, in which two or more HOPO units are encased to satisfy the desired coordination number of metal ions, forming a number of stable chelating rings (chelate effect) that ultimately provides a topology that minimizes steric requirement. The design of these chelators can be modified by introducing extra functionalization of a chelating moiety with another group to improve their efficacy for sensing purposes and interaction with biological sites.

However, the limitations of HOPO-based compounds towards fluorescence sensing and sensitization arise majorly due to their low solubility in most common organic solvents and water media causing them to lack biocompatibility. Further, low quantum yield and comparatively lower photo stability, together with high detection limits, could be the additional constraints that further limit the compounds for efficient sensing. These shortcomings have challenged researchers for new generations of hydroxypyridinones by refining the molecular design for an enhanced selectivity and biocompatibility that could ensure a higher ligand solubility and provide excellent analytical methods for metal detection and quantification with lower detection limits and higher sensitivity. HOPOs are known for their selectivity for Fe^{3+} due to their higher pFe^{3+} values among other dioxo-bidentate ligands.[4] Various other HOPO-based ligands have been reported to form stable complexes with a broad range of metal ions including Al^{3+}, Ga^{3+}, Zn^{2+}, and Mg^{2+} along with lanthanides and actinides. Due to the outstanding iron chelation properties of HOPOs, they have been widely used to treat systematic iron overload diseases, including secondary hemochromatosis and hereditary hemochromatosis.[5] Some HOPO-based ligands have been developed for biological applications following the approval of 3-hydroxy-1,2-dimethyl-4-hydroxypyridinone (deferiprone)

B. K. Kanungo

B. K. Kanungo received an M.Sc. degree from Regional Engineering College (now National Institute of Technology), Rourkela, in 1979, and a PhD degree from Sambalpur University (India) in 1987. He joined as a lecturer in chemistry (1987–1991) at the North Eastern Regional Institute of Science and Technology, Itanagar (India), and moved to Sant Longowal Institute of Engineering and Technology, Longowal (India) as Assistant Professor (1991), subsequently appointed as Professor in 1999. He has been a visiting fellow at the University of Warwick (1999), Coventry (United Kingdom). His research activity spans from synthetic inorganic chemistry to computational modeling of bioinorganic compounds, ligand design, synthesis and solution studies, photochemistry of coordination compounds of transition metals, and lanthanoids.

Minati Baral

Dr. Minati Baral has received her Ph.D. degree (1991) in the field of coordination chemistry from Regional Engineering College Rourkela (Presently NIT Rourkela), Sambalpur University (India). She spent one year (1999–2000) at the University of Warwick, Coventry, United Kingdom as a Commonwealth Postdoctoral Research Fellow. She has been a professor of Chemistry since 2008 and holds the chair of Head, Chemistry Department at National Institute of Technology (NIT), Kurukshetra (India). She also held the post of Dean, Faculty Welfare during 2016–2018 in the same Institution. Her research topics include biomimetics, coordination and supramolecular chemistry, solution thermodynamics, molecular modeling, sensor development, and photochemistry that focused on the synthesis and physical–chemical properties of metal complexes.

as an orally active chelating agent to remove excess iron.[6] HOPOs and their derivatives are known for displaying various pharmacological properties like antifungal, antibacterial, anticancer, antioxidant, and anticonvulsant activities, which play a great role in drug design and discovery.[7,8] They have been immensely used as chelators for diseases like β-thalassemia and other issues linked to the nervous system.[9,10] HOPOs possess clinical applications pertaining to their great affinity towards various biologically relevant metal ions.[11] They possess good affinity for many transition metals, including Fe(II), Fe(III), Zn(II), Cu(II), *etc.* HOPO-based chelator antimicrobial agents have shown better activity towards Gram-negative bacteria and *Acinetobacter* sp.[12] Combining HOPOs with antibiotics was also evaluated for potential clinical application.[13] Synthesis of mono-HOPO derivatives as potential tyrosinase inhibitors has also been reported.[14] HOPO-based metal chelators have also been proven to block virus replication by interacting with the catalytic site of various enzymes.[15,16] Cu^{2+} complexes of HOPO displayed significant activity against *M. tuberculosis*.[17] The antimalarial activity of HOPO derivatives has also been investigated at various times.[18] Some work on the coordination properties of hydroxypyridinone and hydroxypyranone-based chelators has been reported from our laboratory.[19–21] The majority of the work on HOPOs describes their pharmacological applications. Because of these applications, the importance of working on HOPOs has increased with time. Searching 'hydroxypyridinone' as the keyword returned 2358 results in Scopus till 27 November 2023; the inclusion of 'sensor' limited the results to 354, and further confining the search to "review" document type gave only 76, whereas no review was available as fluorescence sensor. The latest review on hydroxypyridinone was reported in 2022.[22] Most reviews focused on the therapeutical applications of HOPOs and other aspects. A review completely dedicated to the sensing properties has not been compiled despite the availability of several papers on the sensing aspect. A chemosensor is generally described as a "molecule of abiotic origin signaling the presence of matter or energy".[23] A receptor is part of a chemosensor that selectively binds with the analyte which leads to a change in the color, structure, fluorescence or electronic properties of the chemosensor. Therefore, chemosensors can sense the analyte and generate an optical or electrical signal. They can be classified into various types, including electrochemical, colorimetric, and fluorimetric sensors. Nowadays, the area of chemosensors is focused on due to their photophysical properties that are susceptible to the environment. They are extensively used to detect heavy metal ions.[24] Although metal ions like Cd^{2+}, Zn^{2+}, Hg^{2+}, Al^{3+}, Cu^{2+} and Fe^{3+} are necessary for various essential processes, including oxygen transport, energy production, *etc.*, these ions can be dangerous to human life if appropriate concentrations are not maintained, leading to diseases like Alzheimer's disease, Wilson's disease, and Minamata disease.[25–27] Metal ion recognition has captured enough attention in the past decades concerning its applications in biology, the environment, green chemistry, catalysis, *etc.*[28,29] Considerable efforts have been made to synthesize versatile yet easy-to-make sensors with high efficiency and sensitivity for different metal ions. The rising demand for chemosensors is due to their selectivity towards various harmful analytes that can be toxic to human beings; hence, they are useful for environmental and industrial sample analysis for monitoring their concentrations. Among other sensing techniques, fluorescent chemosensors are outstanding due to their versatile properties like high temporal and spatial resolution at a very low concentration, thereby playing an important role in *in vivo* imaging applications with high sensitivity and selectivity, quick response and good efficiency with a lower maintenance. They generate a fluorescent signal upon altering the photophysical properties upon binding a specific analyte to a receptor;[30] there could be an enhancement (turn-on chemosensor) or a decrease (turn-off chemosensor) in fluorescence intensity. Functionalized fluorophore-based analytical assays are important in biotechnology, medicinal chemistry, and environmental sciences.[31,32] Fluorescent sensors usually have two major parts: a receptor unit and a fluorophore. The fluorophore transforms information into an optical form by acting as a signaling unit while the receptor recognizes the analyte (Fig. 2). A change in the fluorophore photophysical properties is noticed upon binding of an analyte to the receptor in terms of an optical signal showing enhancement or quenching of fluorescence.[33] Recent developments in fluorescent sensor synthesis and application have become a hotspot in opening up new possibilities for sensing and imaging in various industries, including environmental monitoring, biomedical research, and clinical diagnostics.

HOPO-based fluorescent probes have marked their significant use in detecting intracellular metal ions related to various diseases with metal ion burdens. Lanthanides and actinides are universal in contemporary life and play an essential role in various human-oriented activities, like catalysis, organic light-emitting diodes (OLEDs), clean energy technologies, and lasers.[34–37] Medical applications including Gd(III)-based contrast agents are being used in MRI and β-emitting ^{177}Lu, used for the treatment of gastroenteropancreatic neuroendocrine tumors as approved by the United States Food and Drug Administration.[38,39] Luminescent bio-probes comprising lanthanide complexes impart significant advantages in time-resolved bio-sensing by eliminating background autofluorescence.[40] HOPO-based metal binding moieties bear important characteristics of constructive luminescence sensitization of some lanthanide ions and actinides.[41] The emission properties of these hydroxypyridinone-based chelators are influenced by various fluorescence mechanisms. The quenching mechanism in most of the HOPO-based fluorescent probes is explained due to the formation of metal chelates; this

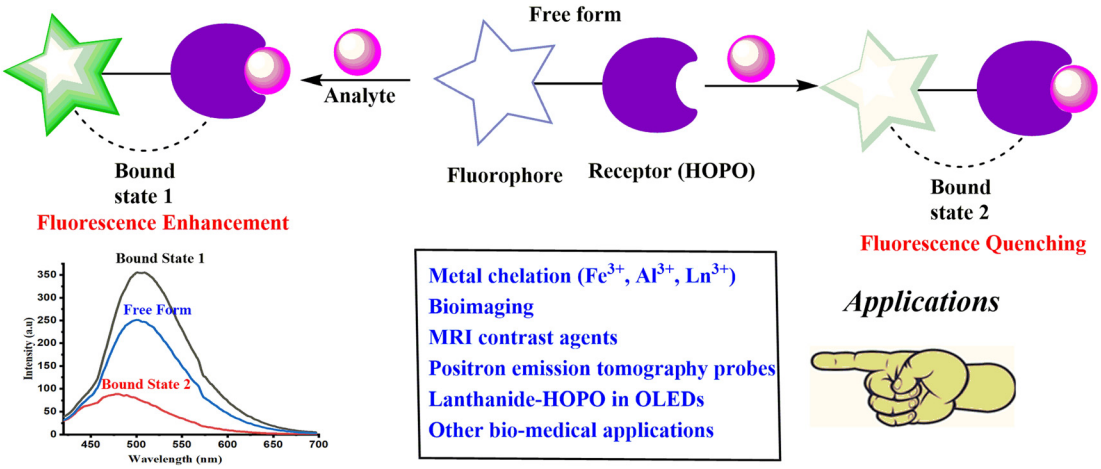

Fig. 2 Schematic representation of a fluorescent chemosensor and its key features.

mechanism is termed chelation-enhanced quenching (CHEQ).[42,43,48] Other mechanisms include aggregation-caused quenching (ACQ),[84] static quenching mechanism,[49] self-quenching mechanism operant in a closely packed solid,[81] electron transfer (PET) process inducing intramolecular fluorescence quenching[60] and energy transfer mechanism.[58] The present review summarizes important chemosensors based on HOPO chelating moieties developed until November 2023 for selective detection of various metal ions. Although much literature is available on hydroxypyridinones, there is less focus on the emission properties of HOPO derivatives and their complexes. The present review concentrates on the sensory aspects of HOPO-based probes and reports various fluorescent and luminescent probes for the selective determination of metal ions, including Fe^{2+}, Cu^{2+}, Mg^{2+}, Zn^{2+}, Fe^{3+}, Gd^{3+}, Tb^{3+}, Eu^{3+}, Cm^{3+} and Sm^{3+}, as well as anions like phosphate and cyanide. The present review provides insight on the research done in the field of fluorescent chemosensors based on hydroxypyridinone binding moieties. Various types of information regarding their emission properties, quenching mechanisms, detection limits, response time, *etc.* have been summarized in this paper. Important applications of hydroxypyridinones due to their selective sensing, versatile chelation, and pharmacological properties are detailed with representative examples. This review has been drafted to comprehend the prominence of the design of the molecule leading for various assets including precise sensing, chelation, stability, and biocompatibility. It will pave the way for different approaches for the design of efficient molecular probes by introducing extra functionalities that provide an improved sensing property and thus can be employed for practical applicability such as in cell imaging, real water sample analysis, *etc.* Taking the above into consideration will result in the development of more significant selective and sensitive chemosensors. The authors believe that the present compilation will help researchers develop new potential compounds incorporating HOPO-based chelating moieties and find them useful for various applications.

HOPO-based fluorescent chemosensors for iron sensing

The intracellular labile iron pool (LIP) is quite toxic despite the biological importance of bounded iron in various processes, including oxygen transport. The Fenton reaction catalyzes oxygen-derived free radical formation due to the redox cycle between its Fe^{2+} and Fe^{3+} stable oxidation states in the presence of reactive oxygen species.[44,45] The reactive radical species cause various problems, such as hepatitis, cancer, and liver cirrhosis. They included dangerous processes like protein oxidation, lipid peroxidation, and DNA lesions due to their interactions with sugars, lipids, proteins, and other biological species.[46,47] To investigate the labile iron

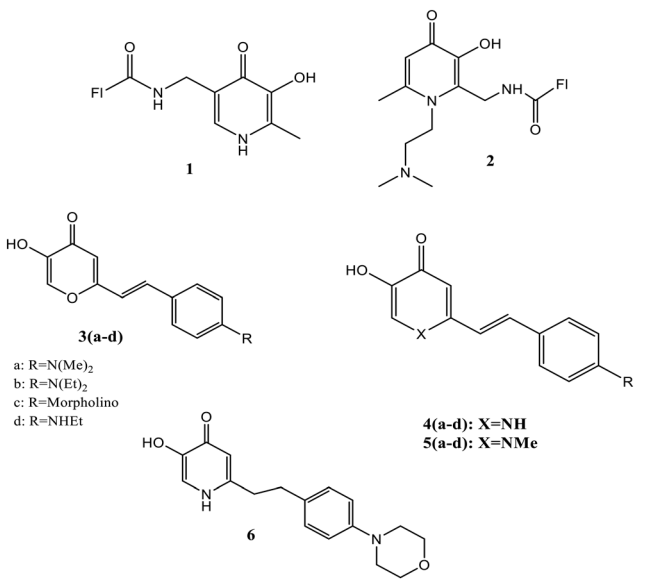

Fig. 3 Structures of fluorescent probes **1**–**6**.

distribution, Fakih *et al.* introduced two fluorescent fluorescein-labeled 3,4-HOPO-based probes (**1** and **2**) [Fig. 3] to monitor iron in endosomal or lysosomal compartments.[48] The study by confocal microscopy and flow cytometry investigated the intracellular distribution and its response to iron concentration modification in murine macrophages, revealing endosomal or lysosomal probe sequestering and its efficient response to vesicular iron concentration modifications. The detection of the cellular quenching and dequenching process displayed a considerable difference in response to the sensor towards intracellular iron concentration manipulations. The fluorophore unit in fluorescein was induced with a quenching effect upon iron binding to the HOPO moiety (Fig. 4). To confirm the probe's selectivity for Fe^{2+}, the interaction of the metal ions *viz.*; Ni^{2+}, Cu^{2+}, Mn^{2+}, Ca^{2+}, Co^{2+}, Mg^{2+}, and Zn^{2+} was recorded in which the expected quenching effect (32.3%) for Cu^{2+}, and fluorescence insensibility toward other metals were observed. Yan and co-workers generated a series of pyridinone or pyranone-based iron chelate fluorescent probes [**3**(**a**–**d**), **4**(**a**–**d**), **5**(**a**–**d**), and **6** (Fig. 3)], which possess an electron donating group substituted aryl ring conjugated to the HOPO.[49] Despite the lower fluorescence properties of HOPO or aryl moieties, the merged structure caused molecules to be fluorescent, as detected by fluorescence spectra. The emission wavelengths lie in the range of 503–560 nm for compounds **3**(**a**–**d**), **4**(**a**–**d**), and **5**(**a**–**d**), while **6** was found to be non-fluorescent in which the HOPO unit was not in conjugation with the phenyl group. The derivative based on pyranone **3**(**a**–**d**) bears a higher emission wavelength. Quenching in fluorescence was observed upon adding iron to the iron-sensitive pyridinone and pyranone fluorescent probes. A linear relationship in fluorescence between Fe^{3+} and the ligand was detected in the concentration ratio of 1 : 3 (Fe : ligand), where the fluorescence was almost quenched in this molar ratio, interpreting the bidentate nature of the chelators. Quenching of metal ions other than Fe^{3+} like Mg^{2+}, Ni^{2+}, Ca^{2+}, Co^{2+}, Fe^{2+}, Mn^{2+}, and Zn^{2+} was also determined; the results of which showed more sensitivity towards Cu^{2+} and Fe^{2+} than other metal ions by two probes. A quenching in fluorescence was also observed for Co^{2+}, Ni^{2+}, and Mn^{2+} when the metal–probe ratio was increased to 100 : 1, while the other metal ions, like Mg^{2+}, Zn^{2+}, and Ca^{2+}, did not show significant quenching. A nonlinear relationship between F_0/F *vs.* $[Fe^{3+}]$ in the Stern–Volmer plot indicated the quenching mechanism as static instead of dynamic.

The loss of fluorescence was observed in the synthesized probes after iron coordination. Further, the pFe^{3+} value of the fluorescent probes confirms the iron chelation. The quantum mechanical calculation methods indicate the more effective binding ability of the probe based on pyridinone than the pyranone-based one.

Non-transferrin-bound iron (NTBI) is defined as the free iron present in plasma, which is formed due to the increasing saturation of transferrin.[50] Two problems are related to its presence, the first being the high affinity of transferrin for iron, which results in low levels of lower molecular weight iron complexes in plasma. Consequently, bacterial infections can be seen more often in iron overload patients as iron is required by the pathogenic bacteria for its growth and replication, and this microbial effect is lost upon saturation of transferrin. Secondly, a distinct uptake system is lacking in NTBI, and transferrin-bound iron is directed to transferrin receptor-expressing cells.[51] Ma and the group presented a fast and easy solution for NTBI measurement in serum.[52] A fluorescent dye attached to a chelating moiety was designed for iron sensing. A systematic investigation was done for effective chelation using different types of chelators like bidentate hydroxypyridinone (**7**), bidentate hydroxypyranone (**8**), hexadentate hydroxypyridinone (**9**), and hexadentate hydroxypyranone (**10**), the structures of which are shown in Fig. 5. Competition studies revealed the capability of HOPO-based hexadentate beads to scavenge maximum low molecular mass and albumin-bound iron. The probes were linked to beads to avoid serum samples'

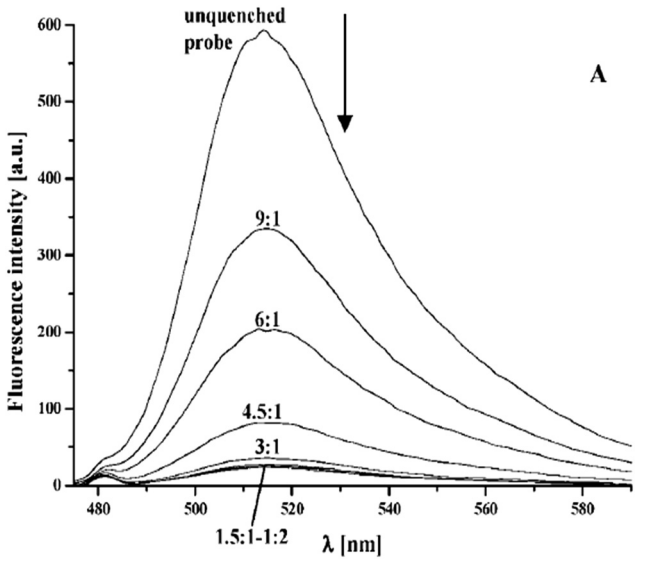

Fig. 4 A representation of the profile of fluorescence emission of probe **2** upon titration with an increase in iron concentration.[48]

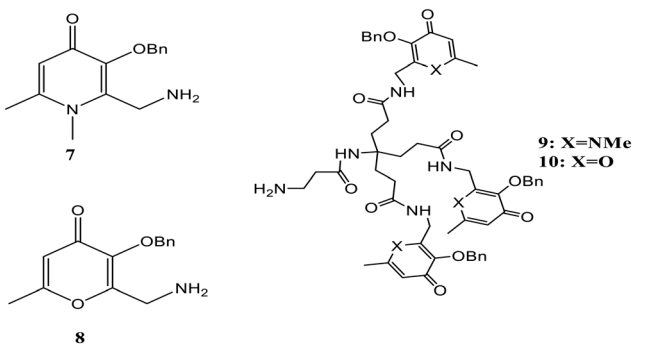

Fig. 5 Structures of the pyridinone and pyranone moieties used as effective chelators.

autofluorescence, and due to the difference in the size between serum proteins and beads, they could be separated and thus excluded from measurement. The quenching of chelating beads' fluorescence in the presence of iron confirmed the sensitivity towards iron. In short, an assay was developed for the NTBI measurement using an Fe-sensitive probe attached to beads. The reported method can potentially be used to record the progress of treatment of thalassemia, bone marrow transplantation, sickle cell anemia, and hemochromatosis.

Biesuz *et al.* described the synthesis of a novel chelating solid phase based on silica, which was obtained by the reaction of *N*-(3′-aminopropyl)-3-hydroxy-2-methyl-4-pyridinone (AHP) with mesoporous silica MCM41 and was modified by reaction with (3-glycidyloxypropyl) trimethoxysilane, for Fe^{3+} sensing.[53] AHP was selected because of the presence of a substituent group of alkyl amine. MCM41, due to its reduced swelling, good mechanical strength, and insolubility in an aqueous medium, was chosen as the solid support. AHP-MCM41@, a new solid-state device, has a total concentration of active sites around 0.4–0.5 mmol g^{-1} in the final material. The color of the solid phase changes to orange-brown upon complexation with trivalent iron. The equilibrium exists at different M : L stoichiometries between the species and is reached within about two hours, inferring fast sorption kinetics. Mimicking of the behavior of AHP molecules in solution by AHP-MCM41@ was shown upon spectral analysis of the solid phase in equilibrium with solutions of different Fe^{3+} concentrations. The color change was obtained in the case of AHP-MCM41@ upon coming into contact with Fe^{3+} in the presence of powerful complexing agents and at neutral pH, making it suitable for Fe^{3+} sensing (Fig. 6).

Ten different Fe-specific fluorescent probes [**11**(**a**–**j**), Fig. 7] were synthesized in which a part of the fluorescent unit was formed by chelating function, making the design of these probes capable of quickly penetrating membranes.[54] Quenching of fluorescence occurred upon adding either equimolar Fe^{3+} or Fe^{2+}, making the probe iron sensitive and potentially measuring the intracellular labile iron pool.

Complete fluorescence quenching was noted in the 3 : 1 molar ratio [chelator : Fe(III)] for all the chelators while the quenching was off where the molar ratio > 3 : 1 [chelator : Fe(III)]. At the same proportion, **11**(**a**) showed less sensitive behavior toward other metals like Ni^{2+}, Co^{2+} and Mn^{2+}. An increase in fluorescence intensity of this probe was observed with metal ions like Zn^{2+}, Ca^{2+}, and Mg^{2+} [Fig. 8]. In the presence of equimolar Zn^{2+}, the fluorescence of **11**(**a**) was increased with a shift in maximum λ_{em} from 464 nm to 430 nm. There was a further rise in fluorescence with increased Zn^{2+} concentration to 1 mM with the same maximum emission wavelength. The lower ionization constants were indicated by the pFe^{3+} and pK_a values of these ligands, thus showing tight iron binding. Similar pFe^{3+} values were observed for **11**(**a**) and **11**(**b**), while these values were slightly higher for ligands containing conjugated rings [**11**(**c**)–(**f**)]. The value for **11**(**g**) decreases upon introducing the carboxyl group on the ring, whereas **11**(**h**) possesses the highest pFe^{3+} values.

A novel fluorescence assay for pFe^{3+} determination was reported by Ma and co-workers,[55] based on the correlations in the presence of iron and the probe between the relative fluorescence and pFe^{3+}. The fluorescent ligand CP645 possesses pFe^{3+} values within the range of 17–23. The study was expanded, in which the fluorescent probe CP691 (Fig. 9) containing a hexadentate hydroxypyridinone was introduced.[56] A maximum emission wavelength at 474 nm

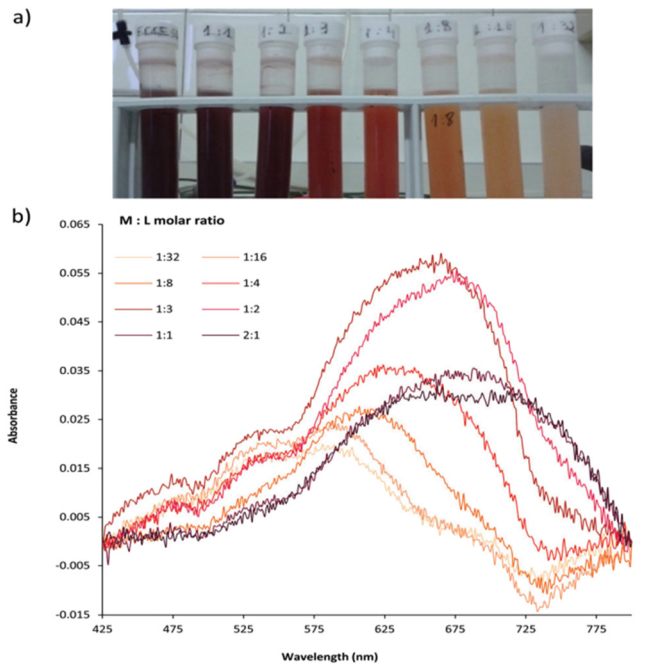

Fig. 6 (a) Colors shown for suspended AHP-MCM41@ at different Fe^{3+}/L ratios. (b) Visible spectra of the solid collected in (a).[53]

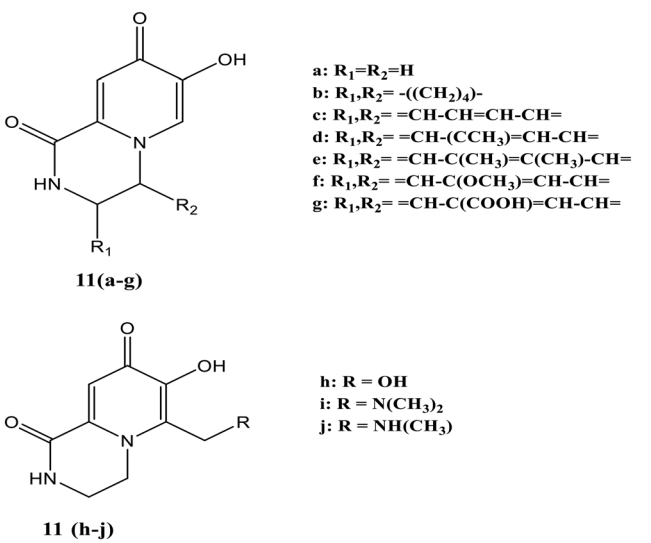

Fig. 7 Structures of iron-specific fluorescent probes **11**(**a**–**j**).

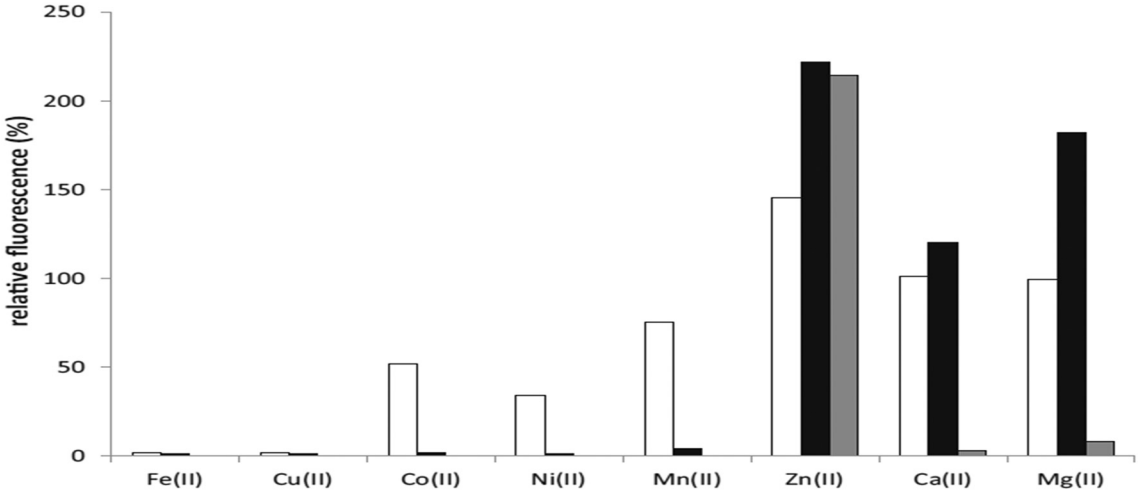

Fig. 8 Quenching of **11**(a) fluorescence for various metal ions.[54]

was noted for iron-free CP691. The presence of iron quenched the fluorescence intensity of CP691, and an excess addition of potent non-fluorescent ligands could recover this fluorescence change. Twelve non-fluorescent chelators with pFe^{3+} values within the range ~20–31 were chosen for the correlation study. As per the thermodynamic considerations, iron could be mobilized from the iron–CP691 complex by the ligands with higher pFe^{3+} values, leading to a more significant fluorescence recovery. Less than 5% of the fluorescence was recovered using weak ligands like EDTA, rhodotorulic acid, and rhizoferrin as the competing ligands at an equivalent amount to CP691. The pFe^{3+} values within the range of 24.5–30.5 using the stronger iron affinity probe CP691 achieved a linear fluorescence response.

Sensing of iron in living systems

Mitochondrial labile iron (LI) contributes significant responsibility in pathologies and oxidative injuries. Presently, an organelle-specific Fe-sensor, which can accurately monitor the labile iron (LI) level in this organelle by exclusively residing in the mitochondria, is unavailable. Abbate *et al.* described the development of precise fluorescent mitochondria Fe-sensors.[57] The family of mitochondria-homing short cell-permeant signal peptides was used as specific iron chelator carriers for the mitochondrial LI evaluation. A prominent compound for synthesizing a set of Fe–chelator peptides was identified using a library of fluorescent peptides based on selectivity for mitochondrial localization. A sensitive response to iron was demonstrated in cell and cell-free systems by synthesizing a panel of iron chelators. Microscopy analysis revealed that in compounds **12**, **13**, **14**, and **15** (Fig. 10), the dansyl [5-(dimethylamino) naphthalene-1-sulfonyl-] group is the leading fluorophore. The iron sensing ability of these chelators was confirmed by fluorescence quenching and dequenching studies in cells and solution. Among all these, compound **14** was found to be the most sensitive toward iron by demonstrating the highest fluorescence quenching.

In further work, selective dual fluorescent iron chelators incorporated in mitochondria-targeted peptides have been designed for the mitochondrial LI pool as biosensors where metal chelating centers and the fluorophore were present on the same structural unit.[58] This fluorescent iron chelator

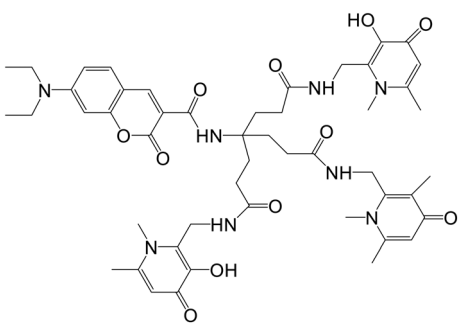

Fig. 9 Structure of probe CP691.

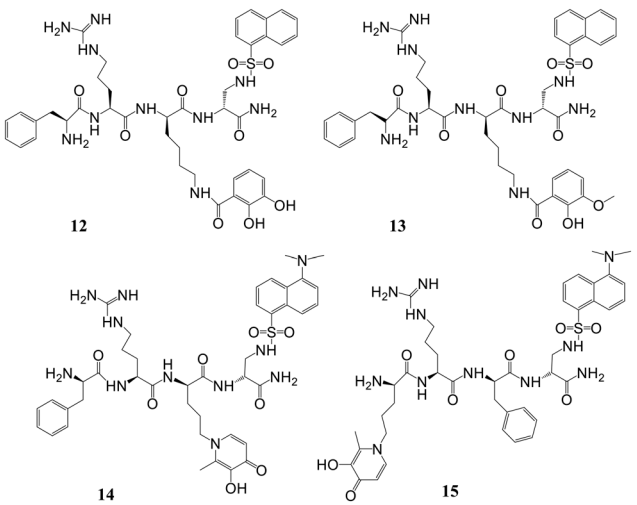

Fig. 10 Structures of mitochondrial-targeted peptides **12**–**15**.

possessed an improved molar extinction coefficient and quantum yield as compared to the dansyl unit, making it a more privileged candidate as an LIP-sensor. Bidentate 3,4-HOPO was adopted for iron scavenging, which has an affinity to bind iron(III) as well as iron(II), leading to the partial Fe(II) chelation at a concentration <10 mM and, thus, capable of sensing Fe(II) levels. The design and preparation of compound **16** was done in isomerically pure form. A panel of probes was prepared where the Phe-residue in the tetrapeptide sequence central part (**18**, **21**–**22**), at the nitrogen-terminus (**19**) or the carbon-terminal lysine (**20**) was replaced by the dual fluorescent probe. A structural analog of **20** was represented by compound **23**, where a protected Fe-chelating moiety (**17**) was incorporated into the structure. Compounds **26** and **27** were designed by the activation of the glutamic acid residue, which was orthogonally protected on the solid support for the selective conjugation of either 1°-(**24**) or 2°-amine (**25**) having HOPO (Fig. 11). The sensitivity of mitochondria-targeted chelators towards iron(III) was determined by the incubation of buffered peptide solutions with the solution of Fe(NTA) complex with an increase in the concentration.

As the Fe(III) levels were increased, continuous quenching in fluorescence emission maxima was noted. Fe(III) chelation seems to play a role here, as the fluorescence intensity of peptide **23** was unaffected by the presence of Fe(III). A progressive decrease in fluorescence was induced upon increment of 1.5 mM Fe(HQ) to **18**-treated cells as compared to untreated control cells. An initial addition of ten mM followed by a twenty mM increase of the deferiprone chelator imparts dequenching of the fluorescent signal, revealing that compound **18** is responsive to the addition of iron and removal from cells. The iron-binding peptides developed in this work impart a better design that can help in the selective delivery of iron probes to mitochondria and measure LIP levels under pathological and physiological conditions.

Four fluorescent probes, out of which three were coumarin-based and the remaining was fluorescein-based, have been reported.[59] The chelating moieties are based either on 3-hydroxypyridin-4-one or 3-hydroxypyran-4-one. These probes (**28**–**31**, Fig. 12) imparted higher selectivity towards iron than other metals like Ni^{2+}, Co^{2+}, Mn^{2+}, Zn^{2+} and Cu^{2+}. Even though copper has a remarkable effect on quenching of fluorescence, its contribution to this study is likely negligible

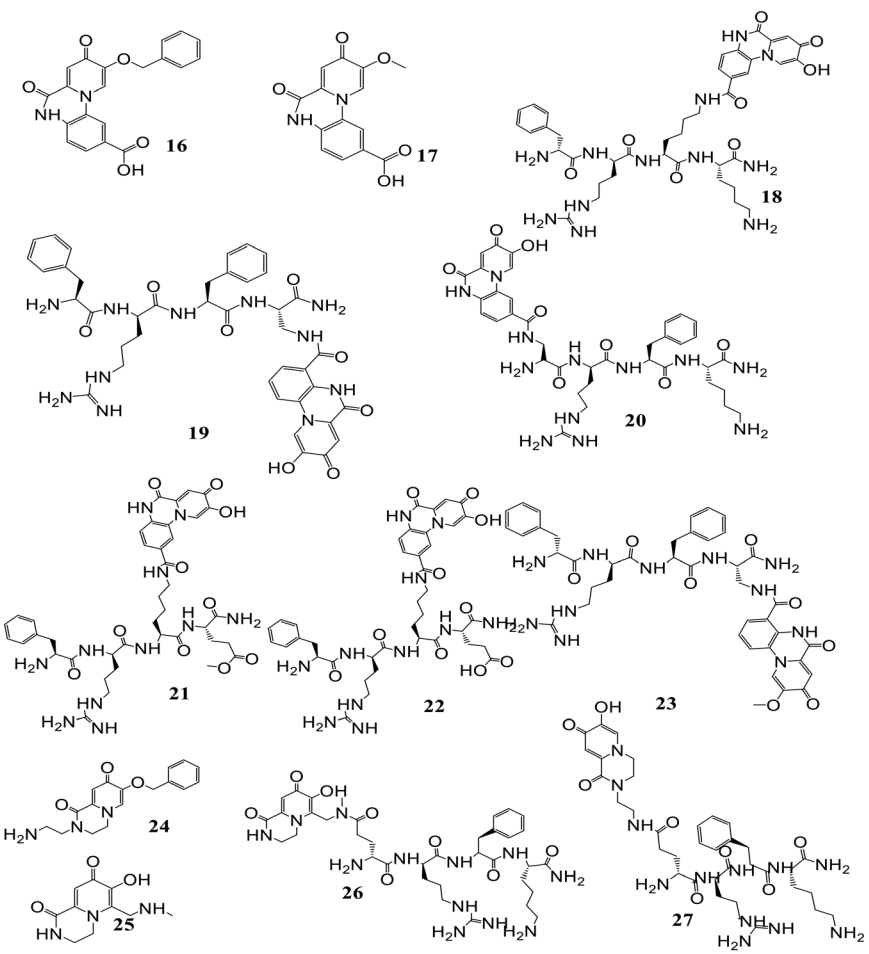

Fig. 11 Structures representing iron chelating peptides and dual fluorescent iron chelators.

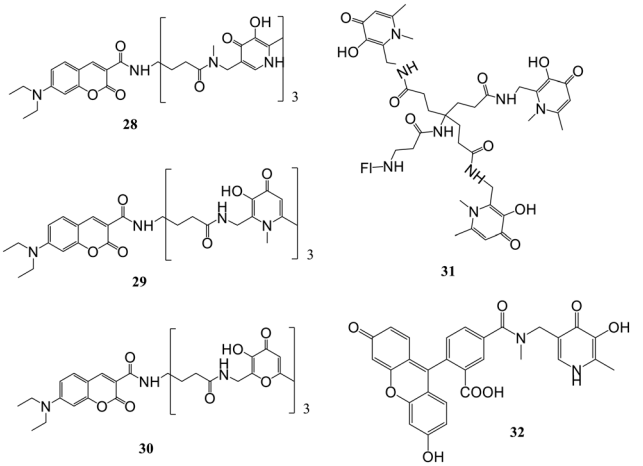

Fig. 12 Structure of iron-sensitive fluorescent probes (**28**–**32**).

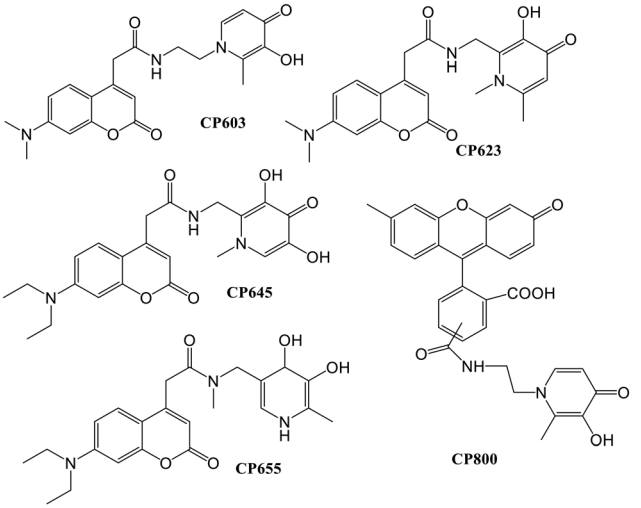

Fig. 13 Fluorescent iron probes loaded in isolated rat hepatocytes.

owing to its relatively low concentration in serum. Further, if the competition by Cu is a problem, the effect of copper on fluorescence quenching could be abolished by the inclusion of *N*,*N*,*N*′,*N*′-tetrakis(2-pyridylmethyl)-ethylenediamine in the assay. The addition of iron only leads to the quenching of fluorescence and does not result in a blue or red wavelength shift. Despite the selectivity of these probes for Fe(III), they were also highly responsive to Fe(II) as after combining with the probes, Fe(II) is immediately oxidized to form Fe(III) complexes. Apart from Fe(II) and Fe(III), quenching of fluorescence also occurred for other metals like Cu(II), Zn(II) and Co(II). No quenching was observed in the case of metal cations like Ca, Na, Mg, and K. Partial quenching of fluorescence occurred in the case of Zn(II), and it bound to the probe, diminishing quenching of fluorescence by Fe(III) as demonstrated by the slope of fluorescence quenching by Zn(II). As the iron affinity studies revealed, pyridone-based hexadentate ligands could compete with all iron from weak ligands like nitrilotriacetic acid and citrate. In fluorescein-based probes, the fluorescence intensity was quantitatively related to the concentration of iron, and the detection limit was 10^{-8} M.

Fakih *et al.* presented work on the development of Fe(III)-sensitive probe SF34 (**32**) having a 3,4-HOPO chelating moiety (Fig. 12) bearing selectivity and high affinity for Fe(III).[60] The sensor in this work highlighted fluorescein as a fluorophore unit and possesses a maximum quenching of fluorescence up to 77.4% upon forming the neutral tris–Fe(III) complex at pH 7.4. The sensor exhibited the characteristic fluorescence properties of fluorescein in an iron(III)-free state. In a cell-free system at pH 7.4, the probe possesses an excitation maximum of 491 nm, and the emission maximum was at 514 nm. At the same time, an effective quenching of sensor fluorescence was noted upon iron(III) binding. The fluorescent probe's physicochemical and living cell properties, mainly accumulated in endosomal or lysosomal compartments, were evaluated. *In vitro*, responsiveness to changes in intracellular iron concentration and iron chelation power of clinically used Fe-chelators were examined using confocal microscopy and flow cytometry. In response to the non-fluorescent high-affinity Fe(III) chelators CP94 and salicylaldehyde isonicotinoyl hydrazone (SIH), dequenching kinetics of complex $Fe(SF34)_3$ were monitored. CP94 showed a fluorescence recovery of 86.9%, while SIH, due to its higher Fe(III) affinity, could recover almost 92.3% of initial fluorescence intensity.

In another study, the iron chelators, which were fluorescent, were loaded into isolated rat hepatocytes, and the determination of the intracellular chelate iron pool of rat hepatocytes was based on the properties of HOPO fluorescent probes (Fig. 13). This iron pool quenched the fluorescence due to an excess in high-affinity iron chelator.[61] This method can detect both the increase and decrease in the iron pool with high sensitivity at a single-cell level. Quenching of fluorescence occurred by adding the 8-HQ–Fe(III) complex but it was dequenched by adding an excess CP94. The intracellular probe concentration was found to be dependent on the partition coefficient in a way that the higher the hydrophobicity of the compound, the higher the intracellular concentration. The fluorescent chelator CP655 was found to be the most sensitive probe to monitor the chelated iron, as revealed by the increase in fluorescence by the addition of CP94.

Detection of other significant metals and anions by HOPO chelators

Most work on hydroxypyridinone-based chelators has been carried out for trivalent iron, lanthanides, and actinides. The use of such ligands as luminescence sensors is scarce. The available data are presented in the following paragraphs.

A 3,4-HOPO-based tripodal ligand **33** (Fig. 14) was designed and developed by Chaves *et al.*[62] The coordination behavior of ligand **33** was studied towards Gd^{3+} and Ga^{3+} through solution thermodynamics. Results from the

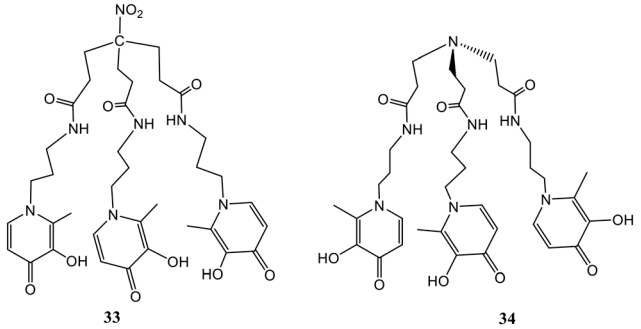

Fig. 14 Structures of 3-4-HOPO-based ligands **33** and **34**.

potentiometric and spectrophotometric titrations suggested the formation of 1 : 1 metal–ligand complexes with the Ga^{3+} complex having higher stability than the Gd^{3+} complex ($\log\beta$ = 14.3 for Gd^{3+} and $\log\beta$ = 26.2 for Ga^{3+}). From the DFT studies, the presence of two water molecules in the coordination sphere of the Gd^{3+}–**33** complex was confirmed, but the rate of water exchange in the Gd^{3+}–**33** complex is slightly lower than the Gd^{3+}–**34** complex which is possibly due to differing charges. However, the Gd^{3+}–**33** complex has high proton relaxivity. Further, the biodistribution studies indicate that the Ga^{3+}–**33** complex showed high *in vivo* stability and rapid renal elimination. Therefore, the Gd^{3+}–**33** and Ga^{3+}–**33** complexes can be potentially used for targeted labelled conjugates including MRI and ^{68}Ga-PET diagnostic medicines respectively. Similarly, a new 3,4-HOPO-based ligand (**34**, Fig. 14) forms highly stable complexes with lanthanides (Ln^{3+} = La^{3+}, Pr^{3+}, Gd^{3+}, Er^{3+}, Lu^{3+}) in aqueous solution.[63] The potentiometric and spectrophotometric studies revealed the formation of 1 : 1 ligand–Ln^{3+} complexes with high stability. The $\log\beta$ values increased from La^{3+} to Lu^{3+} and were found to be 22.86, 25.29, 26.35, 26.77, and 27.53 for the MLH species respectively. The DFT studies suggested the formation of Ln^{3+} complexes having 8 coordination numbers, six 'O' donors from ligand **34**, and the presence of two water molecules in the coordination sphere. Also, ^{1}H NMR and ^{17}O NMR experiments confirmed the presence of two water molecules in the Gd^{3+}–**34** complex showing a high rate of water exchange. The affinity of ligand **34** was also checked towards zinc ions by solution thermodynamics and the results proved that the trans-metallation of the Gd^{3+}–**34** complex is not favored in the presence of Zn^{2+} ions. The Ln^{3+} complexes of ligand **34** can find their potential use as medical diagnostic probes, particularly the Gd^{3+} complex serving as an MRI contrast agent.

Two non-heme Fe(III) complexes, (**35**) and (**36**), were described for selective detection of inorganic phosphate employing 1,2-hydroxypyridinone ligands *via* the indicator displacement assay (IDA).[64] Structures of probes **35** and **36** are shown in Fig. 15. The protection of open coordination sites to prevent μ-oxo dimer formation in aerated solutions was done by weakly coordinating fluorescein. A rapid and selective twenty-fold increase in emission intensity was noticed by the phosphate coordination accompanied by displacement of the fluorescein unit. Fig. 16(a) shows the fluorescence spectra of **35** toward phosphate and the increase in emission intensity. Both the receptors were exceedingly selective for phosphate over pyrophosphate and other competing anions, including halides, nitrate, arsenate, carbonate, and sulfate. The ligands allowed anion recognition by the Fe(III) center by its remaining open coordination sites. Probe **35** was found to be more selective over acetate and bicarbonate than **36**. A higher selectivity for the targeted anion could not be achieved by a more sterically hindered recognition site.

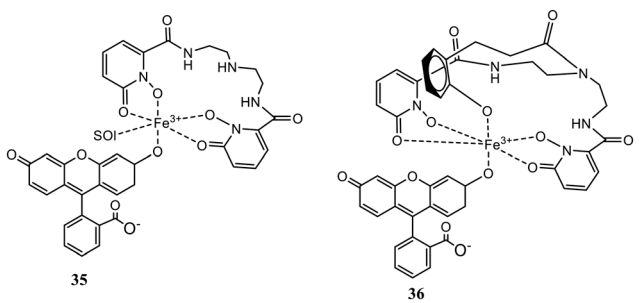

Fig. 15 Structures of iron chelators **35** and **36**.

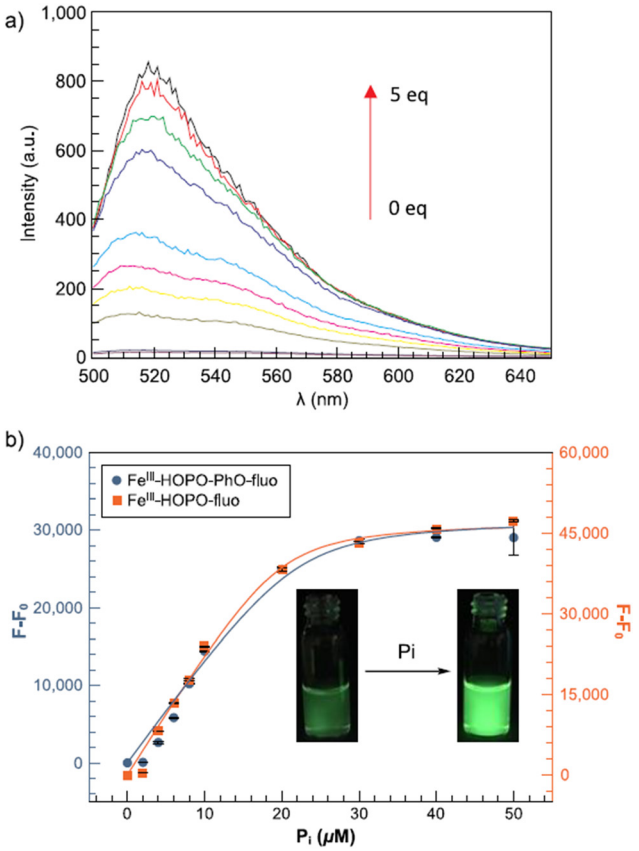

Fig. 16 Fluorescence titration of (**35**) and (**36**) with phosphate (Pi): (a) fluorescence spectra of (**35**) with phosphate; (b) increase in the emission intensity.[64]

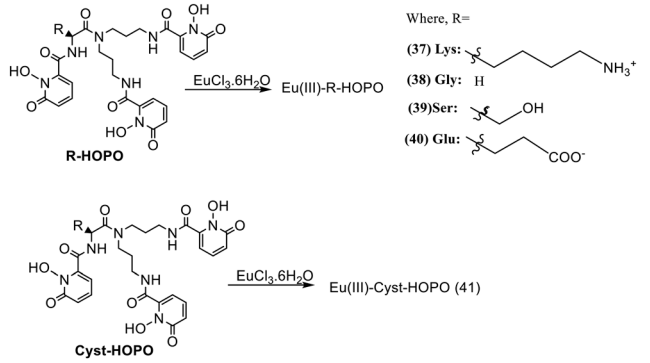

Fig. 17 Structures of Eu(III) probes **37**–**41**.

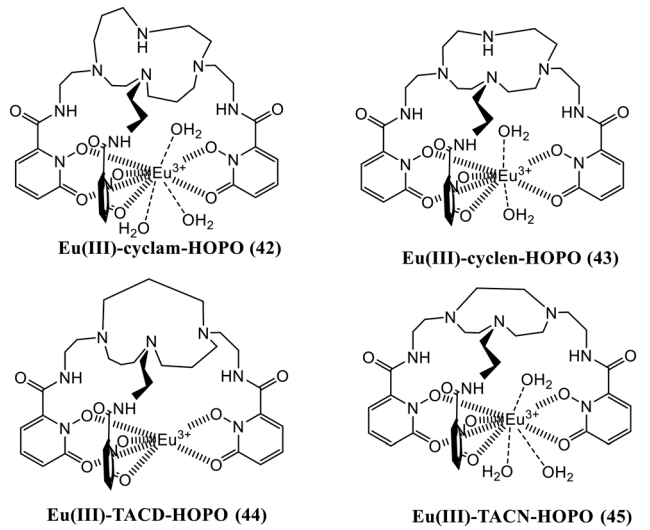

Fig. 18 Structure of Eu(III) complexes **42**–**45**.

The detection limit of the Fe(III) receptors for **35** and **36** was reported to be 3.5 and 4.1 μM, respectively, enabling better phosphate detection of eutrophic water samples. Thus, these fluorescent Fe(III) probes offered an excellent ability to quickly monitor the phosphate level responsible for nutrient pollution in surface water.

Five new Eu^{3+} complexes Eu^{III}-R-HOPO, where R is the amino acid lysine (**37**), glycine (**38**), serine (**39**), glutamic acid (**40**), and cystine (**41**), were designed by Huang *et al.* (Fig. 17), for sensing phosphate ions in water at pH 7.4.[65] On adding ten equivalents of phosphate ($H_2PO_4^-$/HPO_4^{2-}) into each of the complexes, only three showed luminescence changes. The positively charged complex **37**, neutral complex **38**, and **39** enhanced luminescence by five-fold, twenty-fold, and thirty-six-fold, respectively [Fig. 19(a)]. This increase in the intensity is due to the replacement of water molecules, which are directly coordinated with metal center Eu^{3+} by the phosphate ions. The negatively charged complexes **40** and **41** showed no changes in the luminescence in the presence of phosphate ions. Thus, europium compounds **37**, **38**, and **39** are exciting candidates for detecting and remediating phosphate in complicated aqueous media due to their high selectivity, efficacy in water, and significant luminous response.

The increased level of phosphates in the human body leads to a biomedical illness known as hyperphosphatemia. The increased phosphate levels also pollute the environmental water, making it unfit for both aquatic and human life, emphasizing the necessity for developing robust receptors capable of effectively and selectively sequestering the anion from complicated aqueous systems. Four macrocyclic HOPO-based europium(III) probes containing either a cyclam (**42**), cyclen (**43**), TACD (**44**), or TACN (**45**) ligand cap were synthesized (Fig. 18) and reported for their sensing towards phosphate ions.[66] Out of these four complexes, complex **44** has poor water solubility; hence, it could not be evaluated. The remaining three complexes were investigated initially using time-gated luminescence spectroscopy of the europium-centered emission. Complex **43**

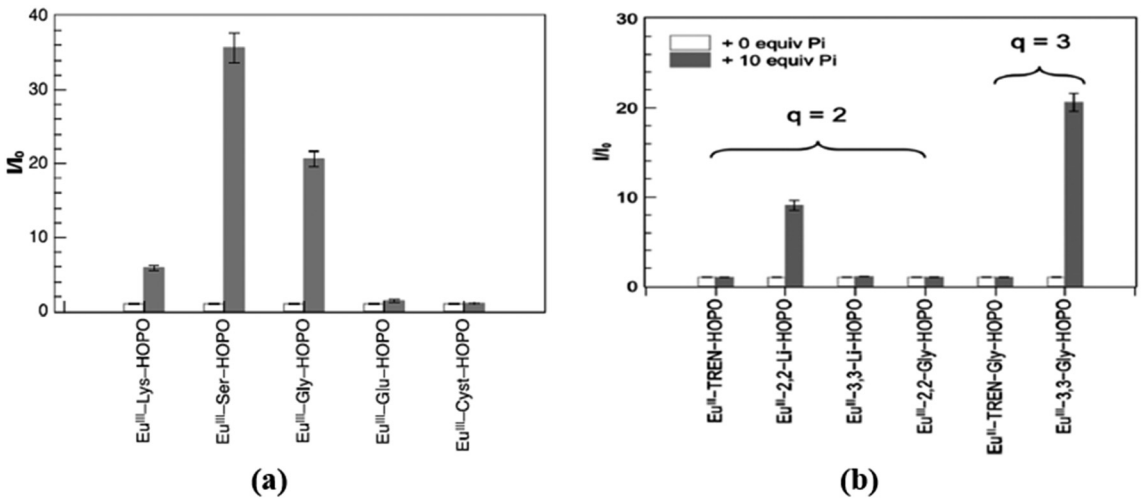

Fig. 19 Changes in the integrated luminescence intensity of Eu-complexes (a) **37**–**41**;[65] (b) **46**–**51** (ref. 67) in the absence (white bars) and presence (grey bars) of ten equivalents of phosphate anion.

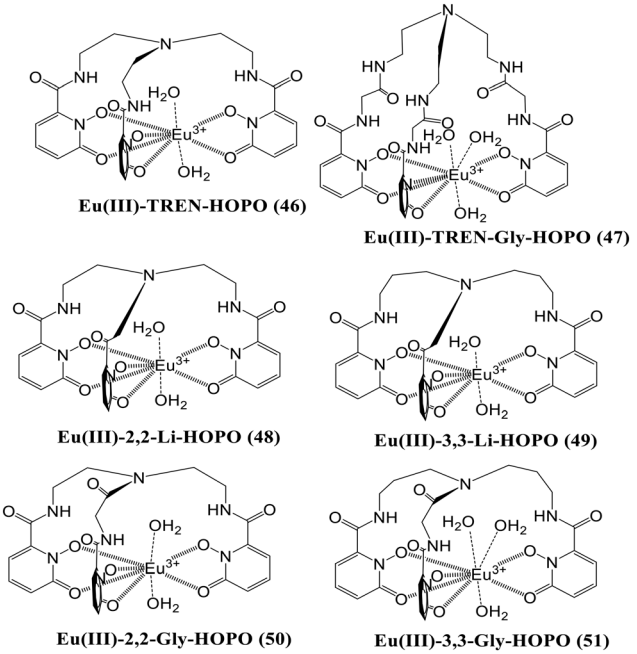

Fig. 20 Structures of Eu(III)-complexes **46**–**51**.

is an eight-coordination complex bearing two water molecules, while complexes **42** and **45** have nine-coordination around the Eu(III) metal having three inner sphere water molecules. Adding ten equivalents of the phosphate anions into the three complexes enhances the luminescence intensity to different extents at 615 nm (λ_{ex} = 334–340 nm). Complex **43** loses one water molecule out of two, resulting in a **43**–Pi ternary complex having a 1 : 1 stoichiometric ratio, whereas the other two complexes, **42** and **45**, lose two water molecules and thus result in the formation of Eu(III)L–Pi_2 complexes having 1 : 2 stoichiometric ratios. All three macrocyclics are selective against other competing anions, particularly bicarbonates and chlorides which are found in higher amounts in the blood; hence, these can be effectively used in treating hyperphosphatemia.

Huang and the group developed another group of 1,2-hydroxypyridonone-based europium(III) complexes (**46**–**51**) that were created (Fig. 20) to test their affinity towards various anions.[67] Complexes **47** and **51** have broader and more flexible ligand caps, which favors the formation of nine-coordination with three water molecules in the inner sphere, whereas the stiffer caps of **46**, **48**, **49** and **50** favor eight-coordination around the Eu(III) center bearing two water molecules in the inner sphere. The luminescence behavior of all six complexes towards different anions was examined in the water medium, and studies revealed that probes **48** and **51** have a strong affinity solely for phosphate ions. In contrast, the other four complexes show no affinity for anions [Fig. 19(b)]. In probe **48** the two water molecules are replaced by two phosphate ions, resulting in a 10-fold increase in the luminescence intensity, whereas all three water molecules are replaced by the phosphate anion in probe **51**, resulting in a twenty-fold rise in luminescence intensity. Thus, both the probes, **48** and **51**, can be used for effectively sensing and sequestering the phosphate anions from the environment and biological systems.

The analysis of the Eu(III) centered complexes **48** and **51** has been further extended to understand the trend in phosphate affinity across the lanthanide series (La–Lu).[68] The sensitization of Eu(III) complexes **48** and **51** through the hydroxypyridinone group formed brightly luminescent ternary complexes Eu(III)-2,2-Li-HOPO-Pi_2 (**52**) and Eu(III)-3,3-Gly-HOPO-Pi_3 (**53**) in the presence of two and three equivalents of phosphate anions respectively. Herein, the authors have developed a series of lanthanide complexes composed of the same ligand and different lanthanides *viz.*, Ln(III)-2,2-Li-HOPO (Ln-**1**) and L(III)-3,3-Gly-HOPO (Ln-**2**) where Ln(III) is La^{3+} to Lu^{3+}. To establish the trend towards phosphate, the receptors Ln-**1** and Ln-**2** are added one after another from La–Lu to probes **52** and **53**, respectively. From the data, it is revealed that in both cases, the affinity of the receptors increases towards the phosphate anion as we go down the series. Hence, the lanthanides coming after Eu^{3+}, having a smaller size than Eu^{3+}, form a more stable complex with the HOPO-based ligands and are capable of sequestering the phosphate anion from both the Eu^{3+}-centered complexes **52** and **53** and water molecules again take the position of phosphate in **52** and **53** resulting in an overall decrease in the time-gated luminescence intensity due to the ternary complexes **52** and **53**. Overall, the authors conclude that the late rare earth lanthanides have higher potential for anion sequestration, particularly lutetium(III), seven orders of magnitude greater than lanthanum(III).

Considering the biological compatibility along with low molecular weight, a mono-substituted naphthalene fluorescent platform was used to covalently bind a chelator moiety, resulting in the development of two new 3,4-HOPO/naphthalene conjugates **54** and **55** (Fig. 21).[69] The naphthalene skeleton is marked in many clinical drugs, as is using naphthalene-based fluorophores to prepare fluorescent sensors. The X-ray analysis confirmed the structures of both compounds as synthesized using traditional heating and microwave irradiation methods. Also, the tautomeric keto forms can be obtained in solution and when the base is present. The tautomeric form and the distance between the fluorescent and chelating functions significantly impact the fluorescence properties of the ligands. Further, **54** was designed such that the fluorophore and the chelating moiety

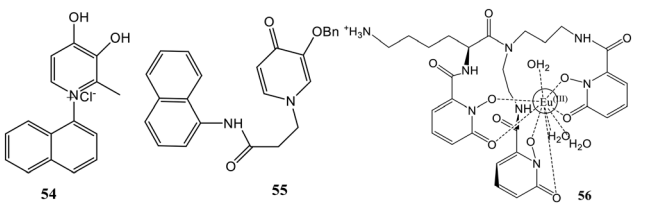

Fig. 21 Structure of **54**, **55**, and **56**.

were directly attached through the N atom of the pyridinone ring, while in **55**, the same functions were separated by the –CH_2CH_2CONH– bridge, thereby generating a more flexible structure. Fluorescence was observed at 450 nm in **54** dihydroxypyridinium in DMSO and ACN, while the keto form showed fluorescence at 365 nm. **54** showed non-fluorescent properties in ethanol, methanol, and water, revealing the fluorescence of **54** in aprotic solvents only. In the case of **55**, the keto form did not exhibit fluorescence, while its dihydroxypyridinium was fluorescent at 340 nm only in DMSO. Therefore, **54** displayed good fluorescence properties and the quenching in fluorescence was observed with variable concentrations of Zn^{2+}, Cu^{2+}, and Fe^{3+}, marking its applicability as an ion sensor. The dependency of fluorescence properties on the naphthalene and the pyridinone distance was thus shown by this distinct fluorescence behavior.

The development of probes is significant for detecting and quantifying cyanide ions due to their high toxicity to the environment and humans. Huang's group presented the development of a luminescent europium probe (Eu^{III}-Lys-HOPO, **56**) that responds to CN^- directly in water (Fig. 21).[70] **56** incorporated a 1,2-HOPO-based sensitizer and a wider ligand cap to favor anion coordination by increasing the number of inner-sphere water molecules. The lysine side arm was used to improve the hydrophilicity of **56**. Characteristic emission spectra with a primary peak at 615 nm were observed when **56** was dissolved in pure water. A nine-fold increase in luminescence intensity in the presence of CN^- is observed in the case of **56** and is found to be hugely selective over other competing anions of environmental relevancy in the presence of Ca^{2+}. This turn-on response was never observed earlier in the case of CN^- probes that function in water. The probe also showed a twelve-, seven-, and two-fold increase for phosphate, carbonate, and fluoride at pH 10.

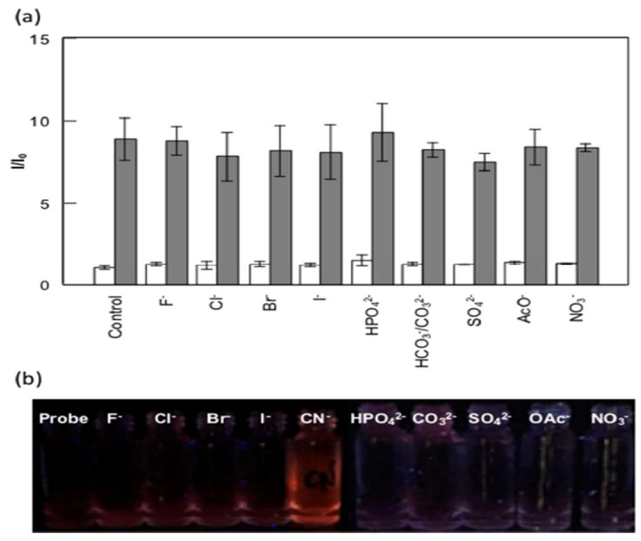

Fig. 22 a) Selectivity of **56** to various environmentally relevant anions. b) Picture showing solutions of **56** in water with corresponding anions and $CaCl_2$ (100 equiv. each) under UV illumination.[70]

Nevertheless, it does not bind Cl^-, Br^-, I^-, $CH_3CO_2^-$, SO_4^{2-}, and NO_3^-. Adding a soluble Ca^{2+} salt such as $CaCl_2$ can eliminate the interference from the competing ions. The competing anions did not affect the CN^- concentration determination in the presence of Ca^{2+}, as demonstrated by the nine-fold increase in metal-centered luminescence upon subsequent addition of a hundred equivalent of CN^-. Fig. 22 depicts the selectivity of **56** towards various environmentally relevant anions and the illumination of **56** solutions in water.

Probes containing HOPO for lanthanide and actinide sensitization

Two-photon-excited fluorescence spectroscopy is a spectroscopic technique to reveal the electronic and structural properties of optically active complexes, molecules, and light–matter interactions.[71] In this work, this spectroscopy is reported as a tool to study the properties of actinide and feature differences between 4f and 5f-series elements.[72] Three chelating moieties with different denticities were used for the same application: (**57**), (**58**), and (**59**) [Fig. 23]. In contrast to the case of lanthanides, it was found that the two-photon absorption properties of the complexes were remarkably affected by the 4f *vs.* 5f nature of metal, and the Cm^{3+} complexes displayed two to three-fold more two-photon absorption cross-sections than the lanthanide analogs with an emission intensity up to 200-fold strong. The results corresponded with the differences in structural and electronic properties between the probed 4f and 5f complexes, and it can be interpreted that this spectroscopy can serve as an essential tool to gain an understanding of the differences between 4f and 5f block elements like the extent of covalency of the ligand–metal bond. In this way, it opened versatile prospects for characterizing scarce compounds. A sharp f–f transition band appeared between 590 and 620 nm of Cm^{3+} when the Cm^{3+}–

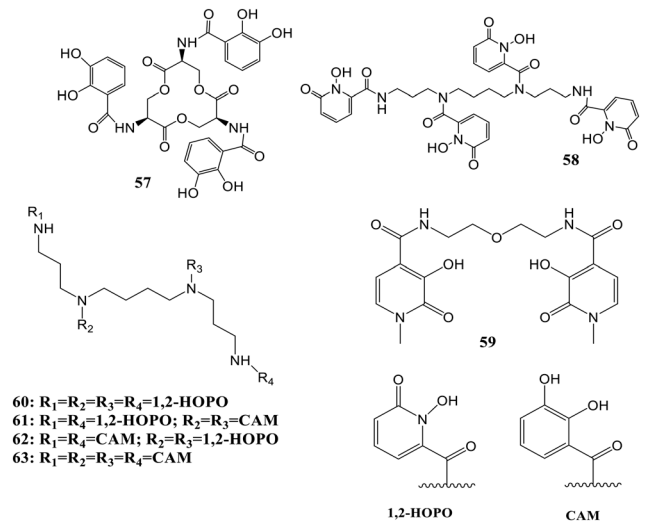

Fig. 23 Structures of probes **57**–**63** used for sensitization of different lanthanides.

58 complex emission spectra were recorded under 684 nm excitation. Sensitization with lower emission intensities resulted when **58** was replaced by enterobactin and **59** due to higher transfer energy efficiency between 1,2-HOPO moieties and Cm^{3+}. The two-photon emission of Cm(III) was also compared with trivalent lanthanides like Tb^{3+} and Eu^{3+} by selecting **58** as the common ligand. Sharp emission bands were noted for Tb^{3+} and Eu^{3+} when the emission spectra for complexes were recorded at pH 7.4 and 684 nm excitation. Excitation spectra of Tb^{3+} and Eu^{3+} complexes were recorded between 680–820 nm, which were very similar to those of Cm^{3+} **58**. All the results interpreted that **58**, excited by two photons, served as the antenna and helped transfer energy to the lanthanides.

In another work, the interaction between the 1,2-HOPO-based hydroxypyridinonate chelator (**58**) and Au^{3+} in solution was characterized, where complexation of the cation with the ligand was observed even at pH 2.2 (acidic) when mostly HOPO binding moieties were protonated.[73] The reported octadentate hydroxypyridinone chelator acts as a therapeutic agent due to non-cytotoxicity at desired dosages and high affinity for f-block elements. The thermodynamic properties of the ligand and Au^{3+} complexes were explored, and the growth of gold nanoparticles by the chelator under specific pH conditions was demonstrated. The complex formation was followed by the reduction of Au^{3+} to Au^{0} with increased pH. At pH 4.9, monodisperse AuNPs were obtained with the 1,2-HOPO-based ligand, which acts as a stabilizing and reducing agent. The sensitization properties of the chelator were exploited for confirmation of the presence of chelator on the metal surface. An emission band at 618 nm was observed for the complex formation between Eu^{3+} and the chelator. The UV-visible spectrum confirmed the aggregation of the particles upon the addition of Eu^{3+}. The chelator can act as both a stabilizing and reducing agent in the growth of particles, as enhancement in fluorescence occurs upon aggregation of particles, and quenching of the emission of fluorophores occurs due to the AuNPs located on their surface. Gold nanoparticle selective aggregation confirms the selectivity towards f-block elements over the lighter elements as the chelator on the Au surface preserved only lanthanides. This new colorimetric assay was reported to be able to reach the detection levels necessary for quantifying lanthanides in industrial waste using the inhibition of the growth of particles by lanthanide elements. This synthesis of gold nanoparticles with a chelator having a good affinity for f-block elements on the surface can pave the way for prospects in therapeutics and biosensing.

Gadolinium ions chelated with linear or macrocyclic ligands are the most common contrast agents employed in about 25% of all MRI processes to enhance image contrast. Several disorders, like consequential nephrogenic systemic fibrosis in patients with renal dysfunction and gadolinium accumulation, have been observed in the healthy person's brain and are related to gadolinium-based contrast agent (GBCA) administration.[74,75] Hence, the tracking of contrast agent excretion through urine after imaging procedures by analytical techniques is necessary for patient safety. Pallares *et al.* reported a luminescence assay to detect GBCAs in urine based on the quenching of probe, Eu^{3+}–**58**, which needs only ten min incubation before measurement.[76] The octadentate chelator, comprised four 1,2-HOPO subunits linked to a central spermine scaffold, was explored for f-block element decorporation. It was investigated for bioassay development emission of several lanthanides, including Eu(III), which can be sensitized by the 1,2-HOPO group. The formation of the Eu^{3+}–**58** complex was prevented by gadolinium-based contrast agents, thereby quenching its emission.

Meanwhile, the chelator Eu(III) complexes sensitized the emission without a contrast agent. The performance of the assay was successfully tested for urine samples of mice. Fig. 24 depicts the optical response of the Eu^{3+}–**58** complex.

A new library of tetrameric peptoid ligands (**60–63**, Fig. 23) containing HOPO or catecholamide chelating moieties linked *via* an ethylenediamine bridge for chelation of f-block metals was synthesized by Ricano and the group using incorporation of high-affinity metal binding moieties to peptoid scaffolds.[77] The mixed ligands sourced from the spermine scaffold were also synthesized for comparison. They proposed to lift the ligand synthesis process by incorporating custom-made sub-monomers with better binding properties of f-elements. Coordination studies based on luminescence for all the ligands were carried out using Tb^{3+} and Eu^{3+}, along with determining stability constants with Eu^{3+} for selected chelators. Considerable differences in photophysical properties and stability of the complex may result from slight variations in ligand structure, as revealed by the studies. Both ligands had more affinity for Ln^{3+} metals with stability constants greater than 10^{29} for Eu(III). 1,2-HOPOs have a

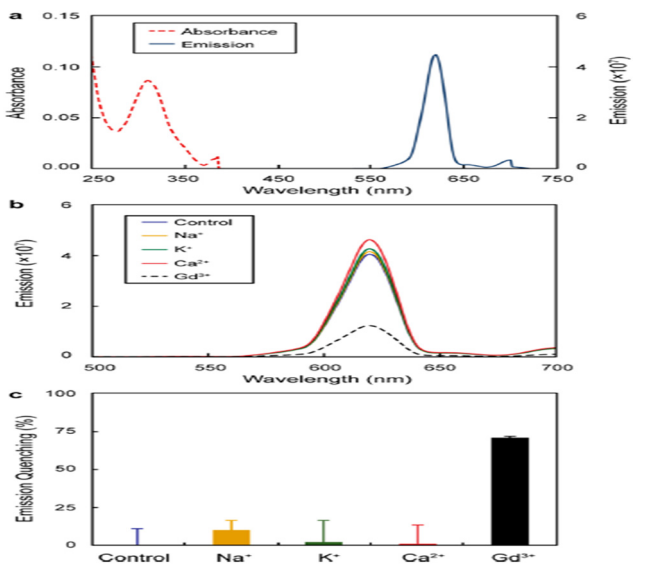

Fig. 24 (a) Absorbance and emission intensity (in a.u) of Eu(III)–**58** (20 μM). (b) Optical response noted for 20 μM complex to 50 μM Gd^{3+} and other cations and subsequent (c) quenching of emission intensity at 620 nm.[76]

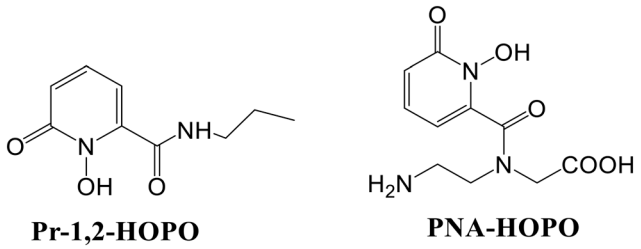

Fig. 25 Structures of bidentate ligands 1-hydroxy-2-(1*H*)-pyridinone-2-carboxylic acid propyl amide (Pr-1,2-HOPO) and PNA-HOPO.

higher attraction towards lanthanides and were found to sensitize Eu^{3+} luminescence. In this work, 1,2-HOPO ligands substitute a nucleo-base pair in a ten-base-pair peptide nucleic acid (PNA) duplex, contributing a solid binding site for Eu^{3+} (Fig. 25).[78] 1,2-HOPO was incorporated into a PNA monomer, which was used to create the binding site for Eu^{3+} in a duplex of peptide nucleic acid. The versatile catalytic and luminescence properties of lanthanides and PNA's affinity to bind towards DNA and RNA made them more fascinating to design optical and MRI sensors. One or three lysine residues were contained at the carbon end of each oligomer (Lys PNA-HOPO or Lys_3 PNA-HOPO, respectively) to advance the solubility of PNA. The binding of Eu^{3+} to ligands containing the 1,2-HOPO moieties of the Lys PNA-HOPO duplex was supported by luminescence studies. When the HOPO unit of Lys PNA-HOPO in solutions was excited at λ = 318 nm, the Eu(III) emission spectrum with a noticeable $^5D_0 \rightarrow {}^7F_2$ emission peak at 614 nm was observed. The spectral data concluded the sensitization of Eu^{3+} luminescence by 1,2-HOPO.

Moore and co-workers reported the unique luminescence properties of 1,2-HOPO-based Eu^{3+} sensitizers.[79] Two octadentate derivatives bearing a pendant amine or a carboxylate group were introduced to allow the conjugation of the complexes with biomolecules of relevance. They found that the photophysical properties of the complexes are greatly affected by the protonation of apical amines. Hugely effective emission with good stability (pEu ~ 20.7–21.8) at pH 7.4 in these complexes was observed in an aqueous solution. Also, at pH ~ 6, the observed intensity is quite decreased due to quenching, which involves the amine backbone protonation, making these complexes bright candidates for applications in homogeneous time-resolved fluorescence assays. The practicability of their utility as long-lived luminescent tags in a bioassay was also demonstrated.

In another work, a series of tetradentate 1,2-HOPO derivatives (**64**), (**65**), and (**66**), as Eu(III) sensitization geometric components have been examined (Fig. 26).[80] Notable differences were observed in the luminescence quantum yield upon alteration of the bridging unit. At pH 7.4 in aqueous solutions, a considerable effect on quantum yield from 21% (aliphatic bridged derivatives) to 6% for $[Eu(\mathbf{66})_2]^-$, apart from affecting the significant triplet excited state, was observed upon the use of the aryl moiety as a bridge. A considerable quantum yield quenching was observed for $[Eu(\mathbf{66})_2]^-$ as compared to $[Eu(\mathbf{65})_2]^-$ which may be attributed to one water molecule in the inner sphere bound to Eu^{3+} while for $[Eu(\mathbf{64})_2]^-$, the low quantum yield may be due to ineffective sensitization of Eu^{3+}. Also, adequate sensitization along with valuable metal-centered emission was shown by the $[Eu(\mathbf{65})_2]^-$ derivative.

1,2-HOPO-based ligands form relatively stable complexes with Eu(III) in an aqueous solution and have proven to be effective sensitizers towards Eu(III). Moore and his group studied the synthesis, structural, and photophysical properties of various Ln(III) complexes formed by using two different bis-bidentate ligands (**67**) and (**68**) with 1,2-HOPO-based chelating moieties (Fig. 27).[81] Fine transitions from the $^5D_0$ excited-state (metal-centered) to ^7F_J ground state multiplet reside in the characteristic emission spectrum of the Eu^{3+} complex.

For transitions J = 1, 2, 3, and 4, maximum intensities were observed at 593, 612, 652, and 702 nm, respectively. The quantum yield for the $[Eu(\mathbf{68})_2]^-$ complex was comparable to $[Eu(\mathbf{67})_2]^-$ at 7.4 pH. Luminescence lifetime was acquired for

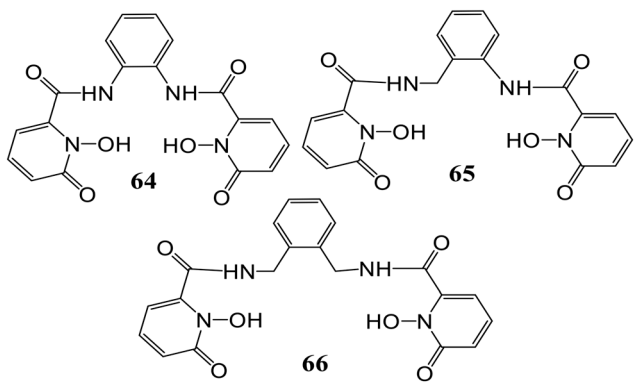

Fig. 26 Structures of the hydroxypyridinone-based ligands examined for Eu^{3+} sensitization.

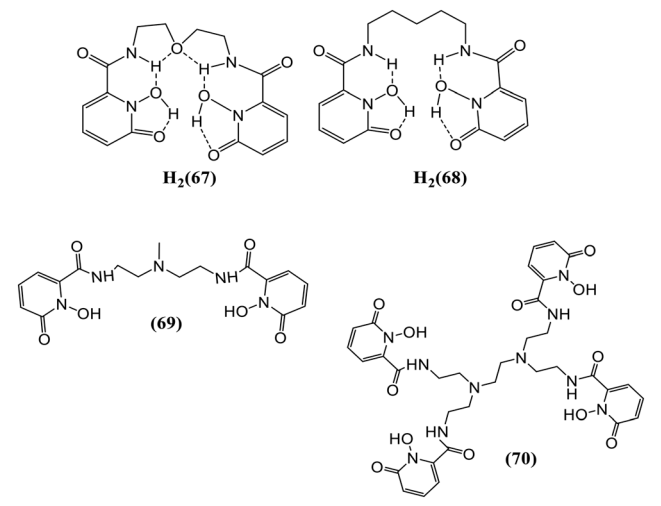

Fig. 27 Structures representing probes **67**–**70**.

both complexes *viz.*, $[Eu(\mathbf{67})_2]^-$ and $[Eu(\mathbf{68})_2]^-$ which were shorter than the measurement of the corresponding solution, which can be ascribed to the self-quenching mechanism in the close-packed solid system. On UV irradiation, a light pink emission was observed for Sm^{3+} complexes of **67** and **68**, showing metal-centered luminescence. The most intense transition at 646 nm corresponds to that from $^4F_{9/2}$ to $^6H_{9/2}$. The sensitization towards other Ln cations, like Tb^{3+} and Dy^{3+} for ML_2 complexes of **67** and **68**, was also measured, but metal-centered luminescence was observed only in the case of Eu(III) and Sm^{3+} complexes. Moore *et al.* have reported the synthesis and photophysical properties of **69** and **70**, as shown in Fig. 27, which employed the 1,2-HOPO chelator as a Eu^{3+} sensitizer.[82] These ligands were found to be thermodynamically stable and exhibit remarkable photophysical properties. **69** was developed as a model for **70**, which, upon dilution in aqueous solutions, forms a complex (ML) with better stability, imparting the vital feature required for the applicability of these complexes towards biological assays. The $[Eu(\mathbf{69})_2]^-$ complex formed by tetradentate (**69**) is stable up to 7×10^{-9} M concentration in an aqueous solution. The octadentate ligand (**70**) imparts improved stability as the $[Eu(\mathbf{70})]^-$ complex upon additional dilution to a limiting concentration of 5×10^{-17} M, the limit of which is outside the minimum detectable concentration of major fluorimeters. Overall, metal-centered luminescence was reduced due to the presence of single coordinated water for $[Eu(\mathbf{70})]^-$. The electronic absorption spectrum of $[Eu(\mathbf{70})]^-$ has a slight red-shift in λ_{max} at 341 nm, which was lower than the $[Eu(\mathbf{69})_2]^-$ complex. The luminescence spectrum of $[Eu(\mathbf{70})]^-$ is representative of that of the Eu^{3+} cation in a low-symmetry environment. Fig. 28 represents the electronic spectra of the complex.

Daumann and co-workers presented the ligand geometry effect on the photophysical properties of Eu^{3+} and Sm^{3+} 1,2-HOPO complexes in an aqueous solution.[83] They prepared a series of ten tetradentate 1,2-HOPO ligands (**71**–**80**, Fig. 29) along with analogous Eu^{3+} and Sm^{3+} complexes with eight coordination. The authors reported the effect of the change of linker backbone length between two

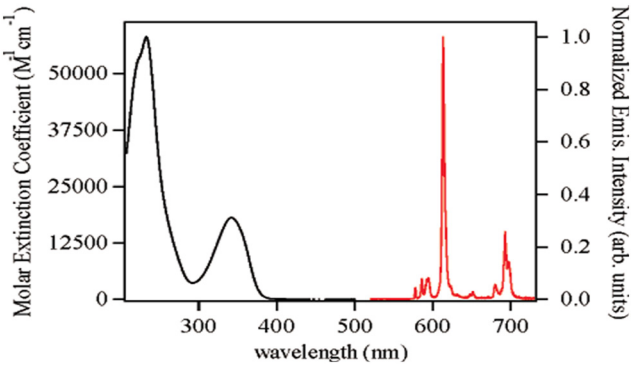

Fig. 28 Figure showing the absorption spectrum in the left and the steady-state emission spectrum in the right.[82]

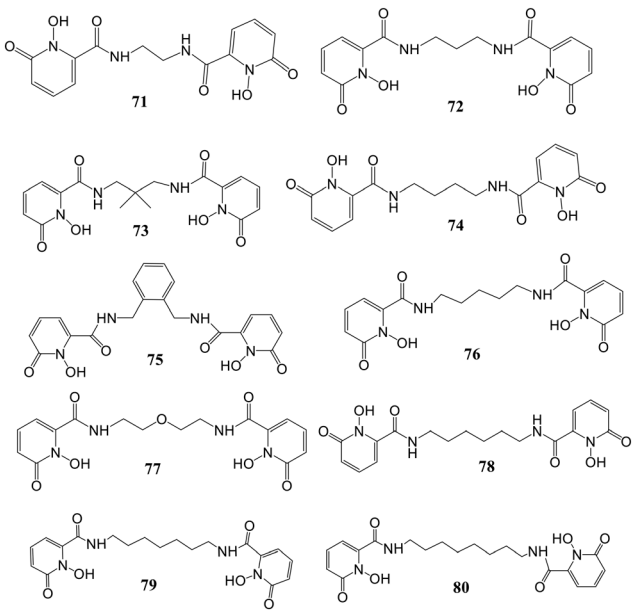

Fig. 29 Structures of tetradentate 1,2-HOPO ligands reported by Daumann and co-workers.[83]

bidentate 1,2-HOPO chelates and the resulting photophysical properties of the complexes. A $[LnL_2]^-$ geometry resulted in the binding of 1,2-HOPO tetradentate ligands to Ln^{3+} (2 : 1). The results interpreted the significance of geometry optimization of the ligand around the lanthanide center for maximizing the transfer efficiency of energy to the Ln center from the organic chromophore for enhancing Φ_{tot}. The fair change in brightness of these mentioned species could be attributed to the effect of the geometry of the chromophore, changed by the aliphatic linker length around the Ln(II) center.

Another group reported a 3,4-HOPO functionalized carbon quantum dots-based probe (HOPO-CQD) for quick detection and monitoring of uranyl ions.[84] The excellent detection performed by this fluorescent probe can be demonstrated by a limit of detection (6.53 ppb) and a shorter response time (30 s). The photoluminescent property of this chemosensor was investigated by fluorescence spectroscopy measurements, which revealed the highest fluorescence intensity at pH 4. The fluorescence intensity of HOPO-CQD was remarkably quenched in the presence of UO_2^{2+} as compared to other ions present. This noteworthy quenching was attributed to the uranyl-specific aggregation of HOPO-CQD resulting in the phenomenon known as aggregation-caused quenching. Also, the inner filter effect was discovered due to the partial overlapping of the fluorescence spectrum with the absorption spectrum of uranyl ions, thereby contributing to the fluorescence quenching.

Other than the HOPO-based chelators, there are some environment-friendly hybrid materials reported for the fluorescence sensing of metal ions. A fluorescent microcapsule probe **81** developed using sporopollenin, ethylenediamine, and BODIPY was reported for selectively

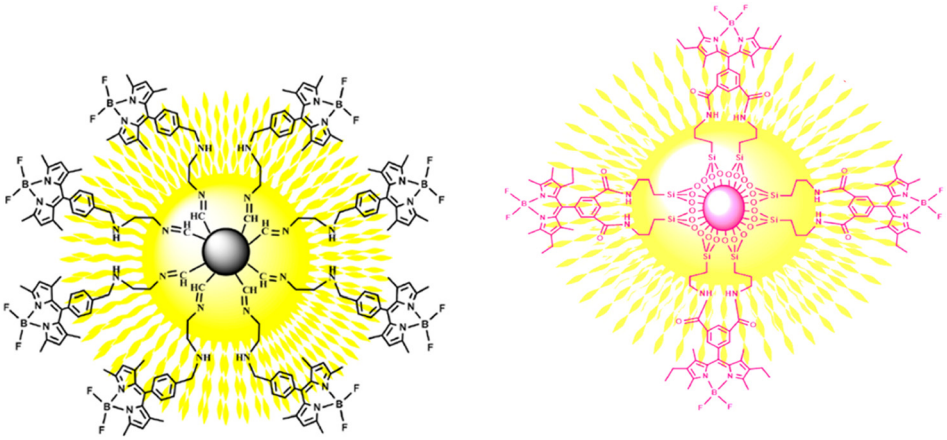

81 82

Fig. 30 Molecular framework of hybrid fluorescent copper sensors **81** (ref. 85) and **82**.[86]

sensing Cu^{2+} ions in water : ethanol medium (70 : 30 v/v).[85] Among various metal ions, the fluorescence of probe **81** was quenched in the presence of Cu^{2+} ions only, with a detection limit of 0.773 μM. The micro capsule **81** is also able to absorb the Cu^{2+} ions and hence can effectively remove them which makes the probe exceptional. Similarly, another hybrid material **82** (Fig. 30) was developed based on BODIPY and f-silica gel for selective recognition of Cu^{2+} ions in an aqueous medium.[86] In the presence of Cu^{2+} ions, a 9-fold quenching in the fluorescence of probe **82** was observed. The detection limit was found to be 4.63 μM. Also, the Langmuir adsorption isotherm was used to study the adsorption behavior of Cu^{2+} ions, resulting in a maximum capacity of 19.920 mg g^{-1}. These results suggest that the hybrid material **82** can be used both as a sensor and an adsorbent for the detection and removal of Cu^{2+} ions from environmental wastes.

Conclusions

This review describes the employment of hydroxypyridinone-based fluorescent sensors reported during the last fifteen years for the selective detection of some alkali metals, iron, alkaline earth metals, lanthanides, and a few anions in biological, environmental, and industrial samples. The lanthanide luminescent probes encompassing hydroxypyridinones as chelation units are also revealed in this review. Despite the excellent selective binding ability and sensitivity towards fluorescence of the hydroxypyridinones, only a few reports showing their utilization as fluorescent probes are available; hence, more attention is needed to explore their optimum employability. While assembling the information for this review, it was observed that the chelators majorly revolved around iron sensing and lanthanide sensitization, with a limited focus on other cations and anions. With various amendments including extra-functionalization, polychelation, *etc.* these chelators could be used to detect other biologically and environmentally significant ions. Fluorescent sensors could be developed which are more centered on *in vivo* applications. The metal–ligand framework could be modified for comparison studies of their impact on emission properties. More fluorescent probes focused on the detection of heavy metal ions like Pb^{2+}, Cr^{3+}, Hg^{2+}, *etc.* could be developed which will impact their applications in the sensing field. To further improve the biological applications of these chemosensors, probes with more solubility in aqueous media should be designed. The focus should be on the probes that can work in less toxic biomimetic and aqueous media. To fully utilize the capability of these sensors, some constraints like developing robust and reliable assays, optimizing the signal-to-noise ratio, and reducing reaction time should be resolved. Regardless of these challenges, the reported probes will serve various practical applications, and the compiled information in this review not only represents the current status but also will help the researchers work in this field, leading to the development and advancement of chemosensors and sensitizers.

Abbreviations

HOPO	Hydroxypyridinone
NTBI	Non-transferrin bound iron
GBCA	Gadolinium-based contrast agents
LIP	Labile iron pool

Conflicts of interest

There are no conflicts to declare.

References

1 M. A. Santos, S. M. Marques and S. Chaves, *Coord. Chem. Rev.*, 2012, **256**, 240–259.
2 S. Chaves, L. Piemontese, A. Hiremathad and M. A. Santos, *Curr. Med. Chem.*, 2018, **25**, 97–112.
3 A. Cilibrizzi, V. Abbate, Y.-L. Chen, Y. Ma, T. Zhou and R. C. Hider, *Chem. Rev.*, 2018, **118**, 7657–7701.

4 R. C. Hider, S. Roy, Y. M. Ma, X. Le Kong and J. Preston, *Metallomics*, 2011, **3**, 239.
5 F. Oliveira, S. Rocha and R. Fernandes, *J. Clin. Lab. Anal.*, 2014, **28**, 210–218.
6 M. A. Santos, A. Irto, P. Buglyó and S. Chaves, *Molecules*, 2022, **27**, 1966.
7 M. Saeedi, M. Eslamifar and K. Khezri, *Biomed. Pharmacother.*, 2019, **110**, 582–593.
8 X. Jiang, T. Zhou, R. Bai and Y. Xie, *J. Med. Chem.*, 2020, **63**, 14470–14501.
9 Z. D. Liu and R. C. Hider, *Med. Res. Rev.*, 2002, **22**, 26–64.
10 T. Zhou, H. Neubert, D. Y. Liu, Z. D. Liu, Y. M. Ma, X. L. Kong, W. Luo, S. Mark and R. C. Hider, *J. Med. Chem.*, 2006, **49**, 4171–4182.
11 J. Burgess and M. Rangel, in *Advances in Inorganic Chemistry*, Elsevier, 2008, vol. 60, pp. 167–243.
12 S. Han, R. P. Zaniewski, E. S. Marr, B. M. Lacey, A. P. Tomaras, A. Evdokimov, J. R. Miller and V. Shanmugasundaram, *Proc. Natl. Acad. Sci. U. S. A.*, 2010, **107**, 22002–22007.
13 C.-F. Zhu, D.-H. Qiu, X.-L. Kong, R. C. Hider and T. Zhou, *J. Pharm. Pharmacol.*, 2013, **65**, 512–520.
14 D.-Y. Zhao, M.-X. Zhang, X.-W. Dong, Y.-Z. Hu, X.-Y. Dai, X. Wei, R. C. Hider, J.-C. Zhang and T. Zhou, *Bioorg. Med. Chem. Lett.*, 2016, **26**, 3103–3108.
15 B. G. Rao, *Curr. Pharm. Des.*, 2005, **11**, 295–322.
16 M. Rostami, H. Sirous, R. Zabihollahi, M. R. Aghasadeghi, S. M. Sadat, R. Namazi, L. Saghaie, H. R. Memarian and A. Fassihi, *Med. Chem. Res.*, 2015, **24**, 4113–4127.
17 L. E. Salsbury, K. N. Robertson, A. J. Flewelling, H. Li, S. J. Geier, C. M. Vogels, C. A. Gray and S. A. Westcott, *Can. J. Chem.*, 2015, **93**, 334–340.
18 G. F. Mabeza, M. Loyevsky, V. R. Gordeuk and G. Weiss, *Pharmacol. Ther.*, 1999, **81**, 53–75.
19 D. Dash, M. Baral and B. K. Kanungo, *ChemistrySelect*, 2021, **6**, 12165–12181.
20 D. Dash, M. Baral and B. K. Kanungo, *J. Mol. Struct.*, 2020, **1222**, 128796.
21 S. Sharma, M. Baral, D. Dash and B. K. Kanungo, *J. Inclusion Phenom. Macrocyclic Chem.*, 2021, **101**, 275–289.
22 M. A. Santos, A. Irto, P. Buglyó and S. Chaves, *Molecules*, 2022, **27**, 1966.
23 *Fluorescent Chemosensors for Ion and Molecule Recognition*, ed. A. W. Czarnik, American Chemical Society, Washington, DC, 1993, vol. 538.
24 N. S. Patil, R. B. Dhake, M. I. Ahamed and U. Fegade, *J. Fluoresc.*, 2020, **30**, 1295–1330.
25 A. C. Ross, *Modern nutrition in health and disease*, LWW, 2012.
26 M. Jaishankar, T. Tseten, N. Anbalagan, B. B. Mathew and K. N. Beeregowda, *Interdiscip. Toxicol.*, 2014, **7**, 60–72.
27 D. Strausak, J. F. B. Mercer, H. H. Dieter, W. Stremmel and G. Multhaup, *Brain Res. Bull.*, 2001, **55**, 175–185.
28 X. Chen, T. Pradhan, F. Wang, J. S. Kim and J. Yoon, *Chem. Rev.*, 2012, **112**, 1910–1956.
29 Y. Ren, X. Chen, X. Li, H. Lai, Q. Wang, P. Zhou and G. Chen, *J. Theor. Biol.*, 2010, **266**, 291–298.
30 J. H. Wang, Y. M. Liu, Z. M. Dong, J. B. Chao, H. Wang, Y. Wang and S. Shuang, *J. Hazard. Mater.*, 2020, **382**, 121056.
31 *Principles of Fluorescence Spectroscopy*, ed. J. R. Lakowicz, Springer US, Boston, MA, 2006.
32 A. P. De Silva, H. Q. N. Gunaratne, T. Gunnlaugsson, A. J. M. Huxley, C. P. McCoy, J. T. Rademacher and T. E. Rice, *Chem. Rev.*, 1997, **97**, 1515–1566.
33 P. R. Dongare and A. H. Gore, *ChemistrySelect*, 2021, **6**, 5657–5669.
34 M. I. Ojovan and W. E. Lee, *An introduction to nuclear waste immobilization*, Elsevier, Kidlington, Oxford, U.K., Waltham, Mass., 2nd edn, 2014.
35 M. S. Hill, D. J. Liptrot and C. Weetman, *Chem. Soc. Rev.*, 2016, **45**, 972–988.
36 F. Zinna, M. Pasini, F. Galeotti, C. Botta, L. Di Bari and U. Giovanella, *Adv. Funct. Mater.*, 2017, **27**, 1603719.
37 A. Fernandez-Bravo, K. Yao, E. S. Barnard, N. J. Borys, E. S. Levy, B. Tian, C. A. Tajon, L. Moretti, M. V. Altoe, S. Aloni, K. Beketayev, F. Scotognella, B. E. Cohen, E. M. Chan and P. J. Schuck, *Nat. Nanotechnol.*, 2018, **13**, 572–577.
38 G. Stevanato, D. J. Kubicki, G. Menzildjian, A.-S. Chauvin, K. Keller, M. Yulikov, G. Jeschke, M. Mazzanti and L. Emsley, *J. Am. Chem. Soc.*, 2019, **141**, 8746–8751.
39 U.S.F.D.A, *Novel Drug Approvals for 2018*, 2018.
40 J.-C. G. Bünzli and C. Piguet, *Chem. Soc. Rev.*, 2005, **34**, 1048.
41 P. W. Durbin, *Health Phys.*, 2008, **95**, 465–492.
42 Y. Ma, W. Luo, P. J. Quinn, Z. Liu and R. C. Hider, *J. Med. Chem.*, 2004, **47**, 6349–6362.
43 N. Kumari, S. Singh, M. Baral and B. K. Kanungo, *J. Fluoresc.*, 2023, **33**, 859–893.
44 F. Vella, *Biochem. Educ.*, 1995, **23**, 115.
45 B. Halliwell and J. M. C. Gutteridge, in *Methods in Enzymology*, Elsevier, 1990, vol. 186, pp. 1–85.
46 A. Gaeta and R. C. Hider, *Br. J. Pharmacol.*, 2005, **146**, 1041–1059.
47 M. Valko, D. Leibfritz, J. Moncol, M. T. D. Cronin, M. Mazur and J. Telser, *Int. J. Biochem. Cell Biol.*, 2007, **39**, 44–84.
48 S. Fakih, M. Podinovskaia, X. Kong, H. L. Collins, U. E. Schaible and R. C. Hider, *J. Med. Chem.*, 2008, **51**, 4539–4552.
49 H. Yan, R. C. Hider and Y. Ma, *Mol. Phys.*, 2019, **117**, 661–671.
50 I. Gosriwatana, O. Loreal, S. Lu, P. Brissot, J. Porter and R. C. Hider, *Anal. Biochem.*, 1999, **273**, 212–220.
51 G. Y. Oudit, M. G. Trivieri, N. Khaper, P. P. Liu and P. H. Backx, *J. Mol. Med.*, 2006, **84**, 349–364.
52 Y. Ma, M. Podinovskaia, P. J. Evans, G. Emma, U. E. Schaible, J. Porter and R. C. Hider, *Biochem. J.*, 2014, **463**, 351–362.
53 R. Biesuz, M. A. Santos, V. M. Nurchi and G. Alberti, *New J. Chem.*, 2018, **42**, 15237–15244.
54 Y. Ma, X. Kong, V. Abbate and R. C. Hider, *Sens. Actuators, B*, 2015, **213**, 12–19.
55 Y. Ma, Y. Xie and R. C. Hider, *Analyst*, 2013, **138**, 96–99.
56 Y. Ma, T. Zhou and R. C. Hider, *Analyst*, 2015, **140**, 3603–3606.

57 V. Abbate, O. Reelfs, R. C. Hider and C. Pourzand, *Biochem. J.*, 2015, **469**, 357–366.
58 V. Abbate, O. Reelfs, X. Kong, C. Pourzand and R. C. Hider, *Chem. Commun.*, 2016, **52**, 784–787.
59 Y. M. Ma and R. C. Hider, *Bioorg. Med. Chem.*, 2009, **17**, 8093–8101.
60 S. Fakih, M. Podinovskaia, X. Kong, U. E. Schaible, H. L. Collins and R. C. Hider, *J. Pharm. Sci.*, 2009, **98**, 2212–2226.
61 Y. Ma, H. de Groot, Z. Liu, R. C. Hider and F. Petrat, *Biochem. J.*, 2006, **395**, 49–55.
62 S. Chaves, K. Gwizdała, K. Chand, L. Gano, A. Pallier, É. Tóth and M. A. Santos, *Dalton Trans.*, 2022, **51**, 6436–6447.
63 A. C. Mendonça, A. F. Martins, A. Melchior, S. M. Marques, S. Chaves, S. Villette, S. Petoud, P. L. Zanonato, M. Tolazzi, C. S. Bonnet, É. Tóth, P. Di Bernardo, C. F. G. C. Geraldes and M. A. Santos, *Dalton Trans.*, 2013, **42**, 6046.
64 S.-Y. Huang and V. C. Pierre, *JACS Au*, 2022, **2**, 1604–1609.
65 S.-Y. Huang, M. Qian and V. C. Pierre, *Inorg. Chem.*, 2019, **58**, 16087–16099.
66 T. L. M. Martinon, M. V. Ramakrishnam Raju and V. C. Pierre, *Inorg. Chem.*, 2023, **62**, 10064–10076.
67 S.-Y. Huang, M. Qian and V. C. Pierre, *Inorg. Chem.*, 2020, **59**, 4096–4108.
68 R. K. Wilharm, S.-Y. Huang, I. J. Gugger and V. C. Pierre, *Inorg. Chem.*, 2021, **60**, 15808–15817.
69 A. M. G. Silva, A. Leite, M. Andrade, P. Gameiro, P. Brandão, V. Felix, B. De Castro and M. Rangel, *Tetrahedron*, 2010, **66**, 8544–8550.
70 S.-Y. Huang and V. C. Pierre, *Chem. Commun.*, 2018, **54**, 9210–9213.
71 M. Rumi and J. W. Perry, *Adv. Opt. Photonics*, 2010, **2**, 451.
72 R. M. Pallares, M. Sturzbecher-Hoehne, N. H. Shivaram, J. P. Cryan, A. D'Aléo and R. J. Abergel, *J. Phys. Chem. Lett.*, 2020, **11**, 6063–6067.
73 R. M. Pallares, K. P. Carter, S. E. Zeltmann, T. Tratnjek, A. M. Minor and R. J. Abergel, *Inorg. Chem.*, 2020, **59**, 2030–2036.
74 T. Grobner, *Nephrol., Dial., Transplant.*, 2006, **21**, 1104–1108.
75 P. Robert, X. Violas, S. Grand, S. Lehericy, J.-M. Idée, S. Ballet and C. Corot, *Invest. Radiol.*, 2016, **51**, 73–82.
76 R. M. Pallares, D. D. An, P. Tewari, E. T. Wang and R. J. Abergel, *ACS Sens.*, 2020, **5**, 1281–1286.
77 A. Ricano, I. Captain, K. P. Carter, B. P. Nell, G. J.-P. Deblonde and R. J. Abergel, *Chem. Sci.*, 2019, **10**, 6834–6843.
78 A. R. De Leon, A. O. Olatunde, J. R. Morrow and C. Achim, *Inorg. Chem.*, 2012, **51**, 12597–12599.
79 E. G. Moore, J. Xu, C. J. Jocher, T. M. Corneillie and K. N. Raymond, *Inorg. Chem.*, 2010, **49**, 9928–9939.
80 A. D'Aléo, E. G. Moore, G. Szigethy, J. Xu and K. N. Raymond, *Inorg. Chem.*, 2009, **48**, 9316–9324.
81 E. G. Moore, J. Xu, C. J. Jocher, I. Castro-Rodriguez and K. N. Raymond, *Inorg. Chem.*, 2008, **47**, 3105–3118.
82 E. G. Moore, C. J. Jocher, J. Xu, E. J. Werner and K. N. Raymond, *Inorg. Chem.*, 2007, **46**, 5468–5470.
83 L. J. Daumann, D. S. Tatum, C. M. Andolina, J. I. Pacold, A. D'Aléo, G. Law, J. Xu and K. N. Raymond, *Inorg. Chem.*, 2016, **55**, 114–124.
84 Z. Zhang, D. Zhang, C. Shi, W. Liu, L. Chen, Y. Miao, J. Diwu, J. Li and S. Wang, *Environ. Sci.: Nano*, 2019, **6**, 1457–1465.
85 A. Bilgic, A. Cimen, A. N. Kursunlu and H. S. Karapınar, *Microporous Mesoporous Mater.*, 2022, **330**, 111600.
86 A. Bilgic, A. Cimen and A. N. Kursunlu, *Sci. Total Environ.*, 2022, **845**, 157170.